Pontifícia Universidade Católica
do Rio de Janeiro

Rodrigo Rolim Mendes de Alencar

1-Bit Quantization Applied to Continuous Phase Modulation

Dissertação de Mestrado

Dissertation presented to the Programa de Pós–graduação em Engenharia Elétrica of PUC-Rio in partial fulfillment of the requirements for the degree of Mestre em Engenharia Elétrica.

Advisor: Prof. Lukas Tobias Nepomuk Landau

Rio de Janeiro
August 2020

Pontifícia Universidade Católica
do Rio de Janeiro

Rodrigo Rolim Mendes de Alencar

1-Bit Quantization Applied to Continuous Phase Modulation

Dissertation presented to the Programa de Pós–graduação em Engenharia Elétrica of PUC-Rio in partial fulfillment of the requirements for the degree of Mestre em Engenharia Elétrica. Approved by the Examination Committee:

Prof. Lukas Tobias Nepomuk Landau
Advisor
Centro de Estudos em Telecomunicações – PUC-Rio

Prof. Rodrigo Caiado de Lamare
Centro de Estudos em Telecomunicações – PUC-Rio

Prof. Max Henrique Machado Costa
Unicamp

Prof. Luciano Leonel Mendes
Inatel

Prof. Marco Antonio Grivet Mattoso Maia
Centro de Estudos em Telecomunicações – PUC-Rio

Rio de Janeiro, August the 14th, 2020

Rodrigo Rolim Mendes de Alencar

Rodrigo is graduated in Communications Engineering at the Military Institute of Engineering (IME), in Rio de Janeiro, Brazil. As a military engineer, He worked for a Brazilian Defense Equipment Manufacturer (IMBEL) in its Electronics and Communications Division. Rodrigo is interested in the following areas: Signal Processing, Embedded Systems, Internet of Things and Software-defined Radios.

Bibliographic data

de Alencar, Rodrigo Rolim Mendes

1-Bit Quantization Applied to Continuous Phase Modulation / Rodrigo Rolim Mendes de Alencar; advisor: Lukas Tobias Nepomuk Landau. – 2020.

82 f: il. color. ; 30 cm

Dissertação (mestrado) - Pontifícia Universidade Católica do Rio de Janeiro, Departamento de Engenharia Elétrica, Centro de Estudos em Telecomunicações, 2020.

Inclui bibliografia

1. Engenharia Elétrica – Teses. 2. Engenharia de Telecomunicações – Teses. 3. Quantização de 1-bit. 4. Modulação de Fase Contínua. 5. Decodificação Iterativa. 6. Sinalização em taxas Faster-than-Nyquist. 7. Amostragem Adaptativa. I. Landau, Lukas Tobias Nepomuk. II. Pontifícia Universidade Católica do Rio de Janeiro. Departamento de Engenharia Elétrica, Centro de Estudos em Telecomunicações. III. Título.

CDD: 621.3

To my parents,
for their support and encouragement.

Acknowledgments

First of all I would like to thank my advisor Prof. Lukas Landau for giving me the opportunity to work on this thesis. With his continuous support and motivation, he has shown his passion towards lecturing and assisting students. More than that, he presents a friendly behavior, striving for meaningful interactions with students and fellow professors. For all above said and for treating with all regard my own ideas onto this research topic, he deserves my sincere gratitude.

I also want to express my gratitude to the professors from CETUC for sharing experience and knowledge during the courses lectures. For this reason, it is worth to mention the professors Raimundo Sampaio Neto, José Mauro Pedro Fortes and, especially, Rodrigo Caiado de Lamare, who has contributed directly and indirectly to this work, with mentorship and paper review.

Furthermore, I want to thank IMBEL for enabling the completion of this thesis by allowing the flexibility of the working hours during this period. More specifically, I want to thank Colonel Marcus Vinícius dos Santos Fernandes for this support, understanding the importance of the master's degree for the career of an engineer.

I am also grateful to the members of my defense committee, Rodrigo Caiado de Lamare, Max Henrique Machado Costa, Luciano Leonel Mendes and Marco Antonio Grivet Mattoso Maia, who generously took their time to evaluate this thesis.

Last but not least, a special thanks goes to my family and all the ones dear to me, for the shared strength-recovering moments of love and laughter.

This study was financed in part by the Coordenação de Aperfeiçoamento de Pessoal de Nível Superior - Brasil (CAPES) - Finance Code 001.

Abstract

de Alencar, Rodrigo Rolim Mendes; Landau, Lukas Tobias Nepomuk (Advisor). **1-Bit Quantization Applied to Continuous Phase Modulation**. Rio de Janeiro, 2020. 82p. Dissertação de Mestrado – Departamento de Engenharia Elétrica, Centro de Estudos em Telecomunicações, Pontifícia Universidade Católica do Rio de Janeiro.

Energy and spectral efficiency are appealing features for military communications and internet of things (IoT). On this thesis, systems and schemes with 1-bit quantization and continuous phase modulation (CPM) are studied and proposed to address the needs for modern and power efficient communications. In this context, oversampling with respect to the symbol duration is promising because the information is conveyed in the phase transitions of the CPM signals, which are not strictly bandlimited. With this, the loss in achievable rate caused by the coarse quantization can be greatly reduced, even for higher order modulation schemes. This study investigates different approaches to enhancing the performance of the proposed system model. A channel coding scheme is designed with a tailored bit mapping, by means of employing a soft-in soft-out (SISO) turbo receiver. CPM waveforms with symbol durations significantly shorter than the inverse of the signal bandwidth are proposed, termed faster-than-Nyquist CPM. Higher oversampling is applied with a sample selection strategy for a nonuniform adaptive oversampling model. Finally, numerical results confirm better performance on bit error rate, spectral efficiency and achievable rate for the proposed methods in comparison with state of the art techniques.

Keywords

1-bit Quantization; Continuous Phase Modulation; Iterative Decoding; Faster-than-Nyquist Signaling; Adaptive Sampling.

Resumo

de Alencar, Rodrigo Rolim Mendes; Landau, Lukas Tobias Nepomuk. **Quantização de 1-bit Aplicada a Sistemas de Modulação de Fase Contínua**. Rio de Janeiro, 2020. 82p. Dissertação de Mestrado – Departamento de Engenharia Elétrica, Centro de Estudos em Telecomunicações, Pontifícia Universidade Católica do Rio de Janeiro.

Eficiência energética e espectral são características importantes para comunicações militares e internet das coisas (IoT). Nesta tese, métodos e sistemas de quantização de 1-bit com modulação de fase contínua (CPM) são estudados e propostos para resolver as necessidades de sistemas de comunicações modernos com baixo consumo energético. Nesse contexto, o método de superamostragem em relação a duração de um símbolo é promissor, pois a informação está contida ao longo da transição de fase de sinais CPM, que não são estritamente limitados em banda. Consequentemente, a perda de taxa alcançável causada pela quantização de 1-bit pode ser reduzida consideravelmente, até mesmo para esquemas com maior ordem de modulação. Este estudo investiga diferentes abordagens para melhorar o desempenho do modelo de sistema proposto. Um esquema de codificação de canal é projetado com mapeamento de bits adaptado ao problema de quantização grosseira, fazendo uso de um soft-in soft-out (SISO) turbo receiver. Formas de onda CPM com duração de símbolo significamente menor que o inverso da banda do sinal são propostas, nomeadas de faster-than-Nyquist CPM. Um fator maior de superamostragem é aplicado com uma estratégia de seleção de amostras em um modelo de amostragem adaptativa. Finalmente, resultados numéricos confirmam melhor desempenho em taxa de erro de bit, eficiência espectral e taxa alcançável para os métodos propostos, em comparação às técnicas recentemente utilizadas.

Palavras-chave

Quantização de 1-bit; Modulação de Fase Contínua; Decodificação Iterativa; Sinalização em taxas Faster-than-Nyquist; Amostragem Adaptativa.

Table of contents

List of figures

List of tables

List of Abreviations

ADC	Analog-to-digital converter
AIR	Achievable information rate
APP	*A posteriori* probability
AWGN	Additive white Gaussian noise
BER	Bit error rate
BCJR	Bahl–Cocke–Jelinek–Raviv
bpcu	Bits per channel use
CPFSK	Continuous phase frequency-shift keying
CPM	Continuous phase modulation
DSP	Digital signal processing
FEC	Forward error correction
FSM	Finite-state machine
FSK	Frequency-shift keying
FTN	Faster-than-Nyquist
IDD	Iterative detection and decoding
IF	Intermediate frequency
IoT	Internet of Things
ISI	Intersymbol interference
LLR	Log-likelihood ratio
MAP	Maximum *a posteriori*
MIMO	Multiple-input-multiple-output
ML	Maximum likelihood
MSB	Most significant bit
MSE	Mean squared Error
OSR	Oversampling Ratio

PAM	Pulse-amplitude modulation
PSD	Power spectral density
RC	Raised cosine
RF	Radio frequency
RHS	Right-hand side
RX	Receiver
SDR	Software-defined radio
SISO	Soft-input soft-output
SNR	Signal-to-Noise Ratio
TX	Transmitter
VCO	Voltage-controlled oscillator

If I have seen further
it is by standing on the shoulders of Giants

Isaac Newton

1 Introduction

With the growth of wireless communications technologies, more and more transceiver architectures have been implementing analog components and functions into the digital domain as digital signal processing (DSP) routines. This trend brings a lot of flexibility to communication systems, such as the ones conceived with the software-defined radio (SDR) technology, which poses high demands on performance of analog-to-digital converters (ADCs).

At the same time, data transmission rates in modern communications have been increasing towards the multi-gigabit order. According to [2], the bottleneck in scaling transceiver hardware architecture to work on multi-gigabit rates becomes the ADC, because high-speed and high-precision ADCs are too costly and not favorable in terms of energy efficiency, since the energy consumption of the ADC scales exponentially with its resolution [3]. One promising approach to overcome the limitation with respect to the ADC power consumption is the 1-bit quantization, i.e., only the sign of the signal is known to the receiver. This coarse quantization is combined with oversampling at the receiver in order to compensate for the losses in terms of achievable rate, even for a noisy scenario [4], an argument that goes in accordance with [5], where oversampling is used to achieve extra bits of resolution.

As in military communications applications, commercial applications, like internet of things (IoT), also demand power efficient devices, that in many cases will function entirely on batteries. A great challenge becomes the achievement of high power efficiency as well as addressing all the requirements for transceiver designs on transmit power, receiver sensitivity, battery autonomy, bandwidth coverage, data rate, security and etc., which demand more technical requisites on hardware, firmware and software. In order to meet those needs, spread spectrum, coding and modulation techniques are employed.

In this context, variations of the continuous phase frequency-shift keying (CPFSK) modulation, or more generically the continuous phase modulation (CPM), are widely applied, since constant envelope modulation techniques are attractive because its use on a communication system relaxes the power amplifier design, regarding its linearity. Once the information is conveyed in the phase or in the frequency, efficient non-linear power amplifiers with limited dynamic range can be considered. High spectral efficiency can be achieved by

using smooth phase transitions, which reduces the out-of-band radiation. In such scenario, the information is implicitly conveyed in phase transitions, which makes the use of oversampling promising in the presence of coarse quantization.

1.1 State of the Art

In [6], where a bandlimited channel is considered, a marginal benefit of 1-bit quantization and oversampling at the receiver in terms of achievable rate has been reported. In [7], a significant gain in terms of the achievable rate has been reported due to oversampling, by using a Zakai bandlimited process [8]. Both studies [6, 7] considered a noiseless channel. However, by considering the capacity per unit cost, it has been shown in [4] that 1-bit quantization and oversampling at the receiver can also be beneficial in a noisy scenario, as it was shown later in [9] for bandlimited channels. The high signal-to-noise ratio (SNR) regime has been considered based on the concept of the generalized mutual information [10], which results in a minor benefit in terms of achievable rate. For a mid to high SNR scenario, an analytical evaluation of a lower bound on the mutual information rate is derived in [11] for a 1-bit quantized continuous-time bandlimited additive white Gaussian noise (AWGN) channel. Later, a practical approach for a 16-QAM system is presented in [12], where filter coefficients are optimized by maximizing the minimum distance to decision thresholds, a concept that is extended for multiple-input-single-output channels in [13]. With respect to multiple-input-multiple-output (MIMO) systems, 1-bit ADCs are attractive due to low-cost hardware and low power consumption per antenna, especially in massive MIMO systems [14, 15], where it can also benefit from oversampling [16], being able to perform channel estimation [17]. In this MIMO context with 1-bit quantization, iterative detection and decoding has been studied in [18] to improve the overall bit error rate performance.

Oversampling and 1-bit quantization have been studied before in combination with continuous phase modulation (CPM) in [19, 20]. CPM signals are spectrally efficient, having smooth phase transitions and constant envelope [1, 21], which allows for energy-efficient power amplifiers. The information is implicitly conveyed in phase transitions, which makes the use of oversampling promising in the presence of coarse quantization at the receiver. The approach presented in [9, 22] shows that the achievable rate of the bandlimited channel is lower-bounded by a truncation based auxiliary channel law. The resulting channel has a finite state memory, where a sequence design is beneficial in terms of achievable rate. The same idea is considered for CPM with 1-bit quantization and oversampling at the receiver in [19], where it is shown how

oversampling increases the achievable rate. Later, more practical approaches were proposed in [20], where the intermediate frequency and the waveform is considered in a geometrical analysis of the phase transitions.

This work aims to further explore the study done in the usage of 1-bit quantization and oversampling at receiver in CPM systems, which consists in a favorable combination that promotes spectral and energy efficiency.

1.2 Overview and Contributions

Chapter 2 introduces a generic CPM system model with a 1-bit ADC at the receiver. The concepts behind the continuous phase modulation is presented with the mathematical description of the CPM signal and its phase term. For a better formulation of the receiving process, the signal suffers a decomposition approach to expose time-independent state transitions, which is important to represent the CPM system as a finite-state channel with well-defined states. In the scenario of 1-bit quantization, the choice of some CPM parameters is key to take advantage of the phase crossings through the quantization levels. To serve as support material for the numerical results of the following chapters, a time-discrete system model is derived.

Chapter 3 provides an information theory background as foundation for the numerical evaluation of the achievable information rate for the CPM system presented in Chapter 2. The achievable information rate can be lower-bounded by considering an auxiliary channel law, which often is much simpler than the computation of the actual achievable information rate. Preliminary results for the achievable rate indicate points of improvement that are explored in the following chapters.

Chapter 4 extends the discrete system model for CPM signals received with 1-bit quantization and oversampling, for a sophisticated coding and decoding scheme. The proposed channel coding method implies the processing of soft information using a BCJR algorithm, which is part of an iterative decoding strategy. Additionally, a sophisticated channel coding scheme is proposed which exploits the special properties of the channel with 1-bit quantization. In summary, the main contributions of this chapter are the following:

- An iterative detection and decoding scheme for CPM systems with 1-bit quantization and oversampling at the receiver;
- A novel phase-state-dependent bit mapping, which is designed for the 1-bit ADC problem;

- A channel coding scheme suited for the bit stream separation into bit sub-channels.

Chapter 5 tries to solve the problem brought by coarse quantization with simplicity by reformulating a low-modulation-order CPM scheme with faster-than-Nyquist signaling rate. The idea is promising because it provides good spectral efficiency with a simple demodulation scheme suitable for the 1-bit quantization problem. The contribution of this chapter includes:

- A novel faster-than-Nyquist CPM waveform design for high spectral efficiency;
- A low complexity receiver scheme in accordance with the 1-bit quantization approach.

Finally, **Chapter 6** opens new possibilities with a nonuniform adaptive oversampling strategy. With higher resolution in time the receiver complexity grows accordingly, but specific sample time instances are more relevant than the others, which can be discarded. A mean squared error (MSE) criterion is used for sample selection. The study of this chapter is carried out with the consideration of a raised cosine frequency pulse for the CPM signals. The contributions of the referred chapter are:

- An adequate model for CPM systems with adaptive oversampling;
- The investigation of an MSE criterion for sample selection in the context of adaptive sampling.

1.3 Notation Remarks

To express probabilities of random quantities we use the simplified notation with $P(\boldsymbol{y}^n|x^n) = P(\boldsymbol{Y}^n = \boldsymbol{y}^n|X^n = x^n)$, where the random quantities are denoted by capital letters and its realizations by lower-case letters. Bold symbols denote vectors, namely oversampling vectors, e.g., $\boldsymbol{y}_k$ is a column vector with M entries, where k indicates the kth symbol in time or rather its corresponding time interval. Sequences are denoted with $x^n = [x_1, \ldots, x_n]^T$. Likewise, sequences of vectors are written as $\boldsymbol{y}^n = [\boldsymbol{y}_1^T, \ldots, \boldsymbol{y}_n^T]^T$. A segment of a sequence is given by $x_{k-L}^k = [x_{k-L}, \ldots, x_k]^T$ and $\boldsymbol{y}_{k-L}^k = [\boldsymbol{y}_{k-L}^T, \ldots, \boldsymbol{y}_k^T]^T$.

2 CPM System with 1-bit Quantization

This chapter covers the fundamental concepts used in this thesis. It describes the base system model, for CPM with 1-bit quantization and oversampling at the receiver, investigated in the next chapters. With emphasis on its phase term, the CPM signal is presented with an analytical expression, used for the derivation of a discrete-time system model description that includes 1-bit quantization and oversampling.

2.1 System Model

At the transmitter side, a CPM modulator can be implemented by using a voltage-controlled oscillator (VCO) driven by a baseband pulse-amplitude modulation (PAM) signal, as shown in Fig.2.1, where the output signal frequency varies around a central frequency f_0, maintaining the phase continuity. As for the receiver side, where the 1-bit quantization is applied, the constituent blocks are detailed in the following sections, after the description of the CPM signal, which is presented first.

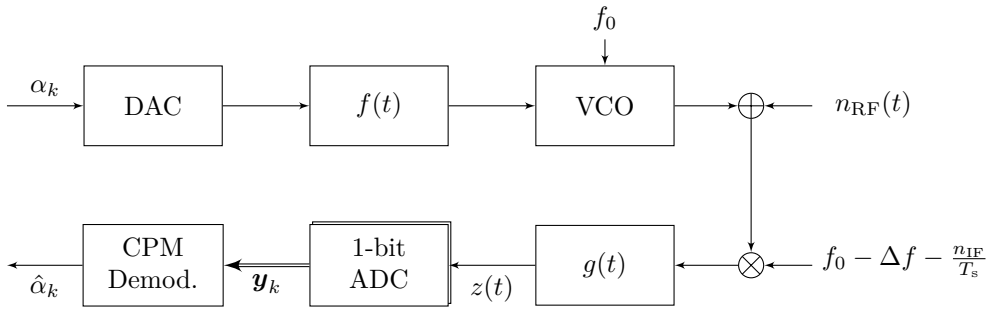

Figure 2.1: System model, continuous phase modulation at a low-IF, with 1-bit quantization and oversampling at the receiver

2.2 Continuous Phase Modulation

The CPM signal in the passband with carrier frequency f_0 [21] is described by

$$s(t) = \mathrm{Re}\left\{\sqrt{\frac{2E_{\mathrm{s}}}{T_{\mathrm{s}}}} e^{j(2\pi f_0 t + \phi(t))}\right\}, \tag{2-1}$$

where $\mathrm{Re}\{\cdot\}$ denotes the real part. The phase term is given by

$$\phi(t) = 2\pi h \sum_{k=0}^{\infty} \alpha_k f(t - kT_\mathrm{s}) + \varphi_0, \tag{2-2}$$

where T_s denotes the symbol duration, $h = \frac{K_\mathrm{cpm}}{P_\mathrm{cpm}}$ is the modulation index, $f(\cdot)$ is the phase response, φ_0 is a phase-offset and α_k represents the transmit symbols with symbol energy E_s. K_cpm and P_cpm must be relatively prime positive integers in order to obtain a finite number of phase states.

The phase response function shapes the phase transition between the phase states. It fulfills the following condition

$$f(\tau) = \begin{cases} 0, & \text{if } \tau \leq 0, \\ \frac{1}{2}, & \text{if } \tau > L_\mathrm{cpm} T_\mathrm{s}, \end{cases} \tag{2-3}$$

where L_cpm is the depth of the memory in terms of transmit symbols. As it is depicted in Fig. 2.2, the phase response corresponds to the integration over the frequency pulse $g_f(\cdot)$, which is conventionally a rectangular pulse, a raised cosine pulse, or a Gaussian pulse. Some of these popular pulse shapes are listed Table 2.1. The notation L_cpmREC and L_cpmRC refers to a rectangular pulse and a raised cosine pulse, respectively, with pulse of length L_cpm symbol intervals, e.g., the 1REC, which is most often referred to as CPFSK, and the 3RC, a raised cosine pulse of length $3T_\mathrm{s}$. The transmit symbols are drawn from an alphabet described by

$$\alpha_k \in \begin{cases} \{\pm 1, \pm 3, \ldots, \pm(M_\mathrm{cpm} - 1)\}, & \text{if } M_\mathrm{cpm} \text{ even}, \\ \{0, \pm 2, \pm 4, \ldots, \pm(M_\mathrm{cpm} - 1)\}, & \text{if } M_\mathrm{cpm} \text{ odd}, \end{cases} \tag{2-4}$$

where M_cpm is the modulation order. Since in digital systems the data is usually binary, the value for M_cpm is often chosen to be a power of 2, i.e., the symbols are associated to distinct binary sequences of the same length.

REC	$g_f(\tau) = \begin{cases} \frac{1}{2L_\mathrm{cpm}T_\mathrm{s}} & , 0 \leq \tau \leq L_\mathrm{cpm}T_\mathrm{s} \\ 0 & , \text{otherwise} \end{cases}$
RC	$g_f(\tau) = \begin{cases} \frac{1}{2L_\mathrm{cpm}T_\mathrm{s}} \left[1 - \cos \frac{2\pi\tau}{L_\mathrm{cpm}T_\mathrm{s}}\right] & , 0 \leq \tau \leq L_\mathrm{cpm}T_\mathrm{s} \\ 0 & , \text{otherwise} \end{cases}$

Table 2.1: Frequency pulse functions $g_f(\tau)$ [1]

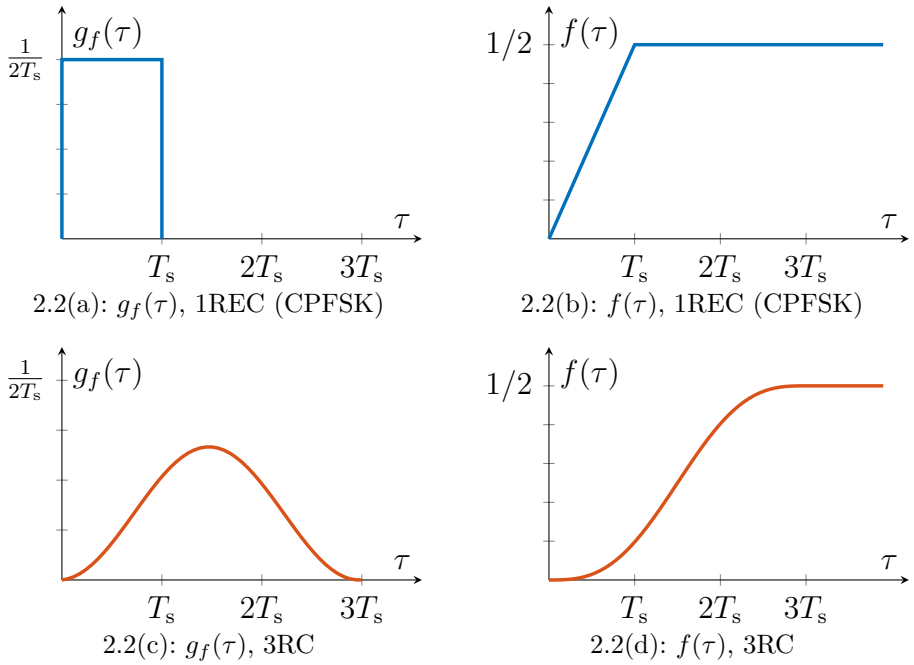

2.2(a): $g_f(\tau)$, 1REC (CPFSK) 2.2(b): $f(\tau)$, 1REC (CPFSK)

2.2(c): $g_f(\tau)$, 3RC 2.2(d): $f(\tau)$, 3RC

Figure 2.2: Frequency pulse shapes $g_f(\tau)$ and their phase responses $f(\tau)$ for 1REC(CPFSK) and 3RC CPM schemes

2.3 Tilted Trellis

Generally, the corresponding phase trellis of (2-2) is time variant, which means that the possible phase states are time-dependent. Because of that, the number of wrapped absolute phase states can be larger than M_{cpm}, e.g., when $M_{\text{cpm}} = 2$ and $h = \frac{1}{2}$, there are at least four trellis states in total and even more depending on the memory of the channel. In order to reduce the complexity at the receiver, a time invariant trellis is constructed by tilting the trellis according to the decomposition approach in [23]. This is illustrated in Fig. 2.3 and Fig. 2.4. The tilt corresponds to an extension of the phase term given by (2-2) as

$$\psi(t) = \phi(t) + \pi h \left(M_{\text{cpm}} - 1\right) \frac{t}{T_s}, \tag{2-5}$$

where the second term on the RHS corresponds to the tilt of the trellis. Taking the derivative of this tilt with respect to time and dividing by 2π results in a frequency offset given by

$$\Delta f = \frac{h(M_{\text{cpm}} - 1)}{2T_s}. \tag{2-6}$$

A modified data sequence is obtained by replacing the symbol notation with the change of variable $x_k = (\alpha_k + M_{\text{cpm}} - 1)/2$, where the corresponding

symbol alphabet can be described with $x_k \in \mathbb{X} = \{0, 1, \ldots, M_{\text{cpm}} - 1\}$. According to [23], substituting $t = \tau + kT_{\text{s}}$ and $\alpha_k = 2x_k - M_{\text{cpm}} + 1$ in equation (2-2) leads to the tilted phase expression within one symbol duration

$$\begin{aligned}\psi(\tau + kT_{\text{s}}) =& 2\pi h \sum_{l=0}^{k-L_{\text{cpm}}} x_l + 4\pi h \sum_{l=0}^{L_{\text{cpm}}-1} x_{k-l} f(\tau + lT_{\text{s}}) \\ &+ \pi h (M_{\text{cpm}} - 1) \frac{\tau}{T_{\text{s}}} \\ &- 2\pi h \left(M_{\text{cpm}} - 1\right) \sum_{l=0}^{L_{\text{cpm}}-1} f(\tau + lT_{\text{s}}) \\ &+ \left(L_{\text{cpm}} - 1\right)\left(M_{\text{cpm}} - 1\right)\pi h + \varphi_0 \quad , 0 \le \tau < T_{\text{s}}.\end{aligned} \tag{2-7}$$

where the time-dependent terms on the RHS depend only on the variable τ, which is well-defined along one symbol duration. Applying the mod 2π operator to the first term on the right hand side of (2-7) yields

$$\begin{aligned}\left(2\pi h \sum_{l=0}^{k-L_{\text{cpm}}} x_l\right) \bmod 2\pi &= \frac{2\pi}{P_{\text{cpm}}} \left(\left(K_{\text{cpm}} \sum_{l=0}^{k-L_{\text{cpm}}} x_l\right) \bmod P_{\text{cpm}}\right) \\ &= \frac{2\pi}{P_{\text{cpm}}} \beta_{k-L_{\text{cpm}}},\end{aligned} \tag{2-8}$$

which introduces the absolute phase state β_k, i.e., it is related to the 2π-wrapped accumulated phase contributions of the input symbols that are prior to the CPM memory. With this, the phase expression for one symbol duration can be fully described by the absolute phase state $\beta_{k-L_{\text{cpm}}}$ and the previous and the current transmit symbols $x_{k-L_{\text{cpm}}+1}^{k}$ given by $\tilde{s}_k = \left[\beta_{k-L_{\text{cpm}}}, x_{k-L_{\text{cpm}}+1}^{k}\right]$. Note that $\tilde{s}_k$ is the appropriate state description for the modeling of the

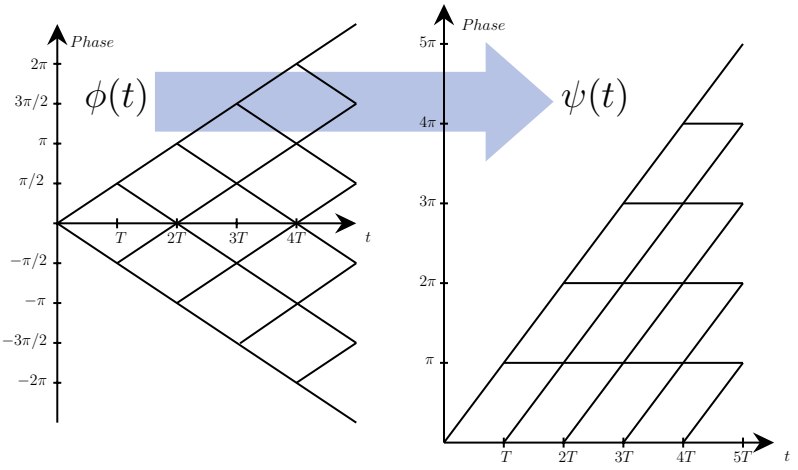

Figure 2.3: CPM trellis (left) and its tilted version (right), $M_{\text{cpm}} = 2$, $h = 1/2$, $\phi_0 = 0$, $L_{\text{cpm}} = 1$ and rectangular frequency pulse

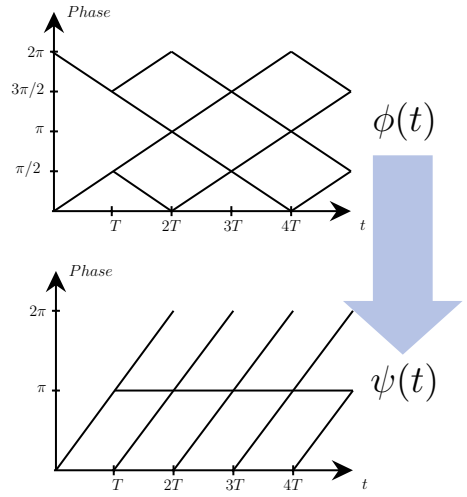

Figure 2.4: CPM wrapped trellis (above) and its tilted version (below)

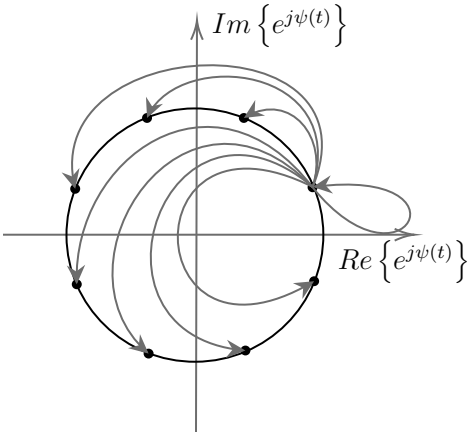

Figure 2.5: $M_{\text{cpm}} = 8$ Constellation diagram of the tilted continuous phase modulation with representation of the state transitions

signal at the intermediate frequency. To model the signal which has passed the bandpass filter at the intermediate frequency another state description, namely s_k will be introduced later. For better integration with 1-bit quantization, $\varphi_0 = \pi h$ is used instead of $\varphi_0 = 0$ whenever it avoids phase states placed on the axis in the constellation diagram, which is the case in all the considered examples. For instance, the constellation of a tilted CPM signal with $M_{\text{cpm}} = 8$ and $h = 1/M_{\text{cpm}}$ can have its phase states and transitions described by Fig. 2.5.

2.4 Low-IF Reception

The tilt of the phase can be established in the actual communication system by receiving at an intermediate frequency (IF). With this, we can consider that different low-IF frequencies can be used, which motivates the

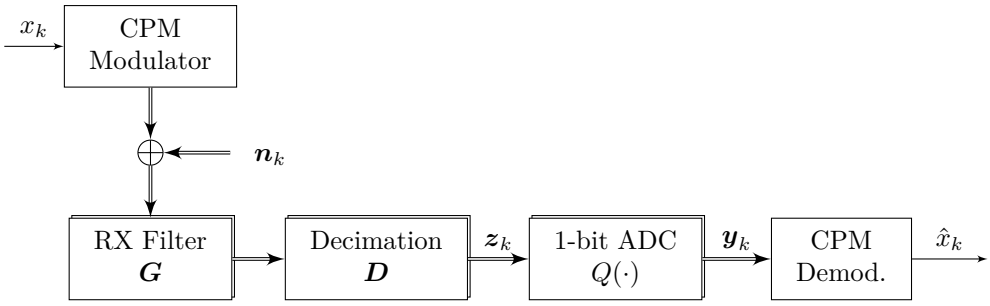

Figure 2.6: Discrete-time description of the CPM system with 1-bit quantization and oversampling at the receiver

definition of

$$\psi_{\mathrm{IF}}(\tau + kT_{\mathrm{s}}) = \psi(\tau + kT_{\mathrm{s}}) + 2\pi \frac{n_{\mathrm{IF}}}{T_s}\tau, \tag{2-9}$$

where $P_{\mathrm{cpm}} \cdot n_{\mathrm{IF}}$ must be a non-negative integer. Choosing $n_{\mathrm{IF}} > 0$ is promising because the appearance of zero-crossings can be adjusted, as proposed in [20]. Therefore, such intermediate frequency is expressed with

$$\left(\Delta f + \frac{n_{\mathrm{IF}}}{T_{\mathrm{s}}}\right) = \frac{h(M_{\mathrm{cpm}} - 1)}{2T_{\mathrm{s}}} + \frac{n_{\mathrm{IF}}}{T_{\mathrm{s}}}, \tag{2-10}$$

where Δf represents the trellis tilt introduced in (2-6). Similarly as in [24], the receiver model contains a complex bandpass filter $g(t)$ with the pass band at the low-IF, which yields an increase of memory in the system by L_g symbols, where $(L_g - 1)T_{\mathrm{s}} < T_g \leq L_g T_{\mathrm{s}}$. The received signal is then given by the convolution of the complex IF signal distorted by additive white Gaussian noise (AWGN) $n(t)$[1] and the complex bandpass filter $g(t)$

$$z\,(t) = \int_{-\infty}^{\infty} \left(\sqrt{\frac{E_{\mathrm{s}}}{T_{\mathrm{s}}}} e^{j\psi_{\mathrm{IF}}(\tau)} + n(\tau)\right) g(t - \tau) d\tau, \tag{2-11}$$

which is sampled with rate $\frac{M}{T_{\mathrm{s}}}$ and quantized with 1-bit resolution in the in-phase component and the quadrature-phase component, where M is the oversampling factor with respect to the transmit symbol duration T_{s}.

2.5 Discrete-time System Model

The discrete-time description presented in Fig. 2.6 implies that the CPM phase should be represented in a vector notation. The corresponding tilted CPM phase $\psi_{\mathrm{IF}}(\tau + kT_{\mathrm{s}})$ for one symbol interval, i.e., $0 \leq \tau < T_{\mathrm{s}}$, is discretized

[1]The statistics of a white noise process are invariant with respect to frequency transformations.

into MD samples, which composes the vector denoted by

$$\boldsymbol{\psi}_k(\tilde{s}_k) = \left[\psi_{\text{IF}}\left(\frac{T_\text{s}}{MD}(kMD+1)\right), \psi_{\text{IF}}\left(\frac{T_\text{s}}{MD}(kMD+2)\right), \ldots, \psi_{\text{IF}}\left(T_\text{s}(k+1)\right)\right]^T,$$

where M is the oversampling factor, and D is a higher resolution multiplier. In order to express a subsequence of $(\eta+1)$ oversampling output symbols, the receive filter $g(t)$ is represented in a matrix form with $\boldsymbol{G}$, as a $MD(\eta+1) \times MD(L_g+\eta+1)$ Toepliz matrix described as follows

$$\boldsymbol{G} = \begin{bmatrix} \left[\ \boldsymbol{g}^T\ \right] & 0\cdots & 0 & 0 \\ 0 & \left[\ \boldsymbol{g}^T\ \right] & 0\cdots 0 & 0 \\ & \ddots\ \ddots\ \ddots & & \\ 0\cdots & 0 & \left[\ \boldsymbol{g}^T\ \right] & 0 \end{bmatrix}, \tag{2-12}$$

where

$$\boldsymbol{g}^T = \sqrt{\frac{T_\text{s}}{MD}}\left[g(L_gT_\text{s}), g\left(\frac{T_\text{s}}{MD}(L_gMD-1)\right), \ldots, g\left(\frac{T_\text{s}}{MD}\right)\right],$$

and unit energy normalization is considered with $\int_{-\infty}^{\infty} g(t)^2dt = 1$ and $\|\boldsymbol{g}\|_2^2 = 1$. Once the CPM signal is not strictly bandlimited, the higher sampling grid adopted permits the model to consider the aliasing effect properly. Consequently, the filtered samples are decimated to the vector $\boldsymbol{z}_{k-\eta}^k$ according to the oversampling factor M, by multiplication with the D-fold decimation matrix $\boldsymbol{D}$ with dimensions $M(\eta+1) \times MD(\eta+1)$, described by

$$D_{i,j} = \begin{cases} 1 & \text{for } j = (i-1)D+1, \\ 0 & \text{otherwise.} \end{cases} \tag{2-13}$$

Then, the result $\boldsymbol{z}_{k-\eta}^k$ is 1-bit quantized to the vector $\boldsymbol{y}_{k-\eta}^k$. All these operations can be represented by the following equations

$$\begin{aligned} \boldsymbol{y}_{k-\eta}^k &= Q\left(\boldsymbol{z}_{k-\eta}^k\right) \\ &= Q\left(\boldsymbol{D}\ \boldsymbol{G}\left[\sqrt{\frac{E_\text{s}}{T_\text{s}}}e^{\boldsymbol{\psi}_{k-\eta-L_g}^k} + \boldsymbol{n}_{k-\eta-L_g}^k\right]\right), \end{aligned} \tag{2-14}$$

where the quantization operator $Q(\cdot)$ is applied element-wise. The quantization operator applied to the vector $\boldsymbol{z}_k$ is described by

$$y_{k,m} = \text{sgn}(\text{Re}\{z_{k,m}\}) + j\text{sgn}(\text{Im}\{z_{k,m}\}),$$

where m denotes the oversampling index that runs from 1 to M and $y_{k,m} \in \{1+j, 1-j, -1+j, -1-j\}$. The vector $\boldsymbol{n}_{k-\eta-L_g}^{k}$ contains complex zero-mean white Gaussian noise samples with variance $\sigma_n^2 = N_0$.

3 Achievable Information Rate

Achievable information rate (AIR) is determined by the number of information bits per symbol that can be transmitted through a given channel reliably. In this context, AIR relies on the mutual information definition measured between the input and output processes of the considered channel. The channel capacity concept, developed by Shannon in [25], is the largest AIR for which exits a coding scheme that can, in principle, achieve any arbitrarily small error probability by choosing a block length sufficiently large. For a given communication system, the channel capacity can be achieved by maximizing the AIR with an optimized input distribution. For CPM systems, an optimization strategy based on a Markov source model is explored in [26]. Later in [19], a scenario with 1-bit quantization is considered with respect to an auxiliary channel law, which is presented in this chapter.

This chapter consists of the study of information rates on the system model presented in the chapter 2.

3.1 Information Theory Background

This section covers some concepts on information theory that are relevant for the evaluation of the AIR for the considered system model.

3.1.1 Mutual Information

According to Shannon in [25], mutual information is described by the amount of information obtained about one random variable or process by observing another random variable or process. In a communication system with two random processes, input X and output $\boldsymbol{Y}$, it is desirable to achieve as much mutual information as possible, i.e., when $\boldsymbol{Y}$ is observed, the amount of information collected from the observation should be enough to reconstruct the input X with certain accuracy, otherwise the communication wouldn't be reliable. In terms of entropy, which is the amount of information contained in

a message often measured in bits, the mutual information can be defined as

$$\begin{aligned} I(X;\boldsymbol{Y}) &= H(X) + H(\boldsymbol{Y}) - H(X,\boldsymbol{Y}) \\ &= H(X) - H(X|\boldsymbol{Y}) \\ &= H(\boldsymbol{Y}) - H(\boldsymbol{Y}|X). \end{aligned} \tag{3-1}$$

By using the entropy definition, the expression from above can rewritten with respect to the probability distributions $P(x)$, $P(\boldsymbol{y})$ and the joint probability distribution $P(x,\boldsymbol{y})$, as follows

$$I(X;\boldsymbol{Y}) = \sum_{\boldsymbol{y}\in\mathbb{Y}}\sum_{x\in\mathbb{X}} P(x,\boldsymbol{y}) \log_2\left(\frac{P(x,\boldsymbol{y})}{P(x)P(\boldsymbol{y})}\right). \tag{3-2}$$

3.1.2 Information Rates

The concept of mutual information rate, or only information rate, describes the mutual information exchange between the processes X and $\boldsymbol{Y}$ per unit of time, i.e., a throughput measurement. Thus, by considering the symbol period and the finite alphabet random processes, the information rate is computed by averaging the mutual information of the symbol based sequences X^n and $\boldsymbol{Y}^n$, which is given by

$$\begin{aligned} \overline{I}(X_k;\boldsymbol{Y}_k) &= \lim_{n\to\infty}\frac{1}{n} I(x_1,\ldots,x_n;\boldsymbol{y}_1,\ldots,\boldsymbol{y}_n) \\ &= \lim_{n\to\infty}\frac{1}{n} I(X^n;\boldsymbol{Y}^n), \end{aligned} \tag{3-3}$$

where n is the length of the input and output sequences. The information rate can also be written as a function of the entropy rates by using (3-1) with

$$\overline{I}(X_k;\boldsymbol{Y}_k) = \overline{H}(X_k) + \overline{H}(\boldsymbol{Y}_k) - \overline{H}(X_k,\boldsymbol{Y}_k). \tag{3-4}$$

3.1.3 Information Rates for Finite-State Channels

The memory brought by the CPM waveform and the receive filter in the system model considered in the previous chapter, permits the channel to be modeled as a finite-state machine (FSM), where current state realizations depend on the previous ones. In such a scenario, the information is conveyed in sequences, which implies that for the evaluation of the information rate, sequences shall be considered.

Assuming that the considered processes are stationary and ergodic the

Shannon-McMillan-Brieman theorem states the following on the entropy rate

$$\overline{H}(X_k) = \lim_{n\to\infty} -\frac{1}{n}\log_2 P(x^n). \tag{3-5}$$

With this, the information rate given in (3-4) can be expressed with

$$\begin{aligned}\overline{I}(X_k;\boldsymbol{Y}_k) &= \lim_{n\to\infty}\left(-\frac{1}{n}\log_2 P(x^n) - \frac{1}{n}\log_2 P(\boldsymbol{y}^n) + \frac{1}{n}\log_2 P(x^n,\boldsymbol{y}^n)\right)\\ &= \lim_{n\to\infty}\left(-\frac{1}{n}\log_2 P(\boldsymbol{y}^n) + \frac{1}{n}\log_2 P(\boldsymbol{y}^n|x^n)\right),\end{aligned} \tag{3-6}$$

where the right-hand side of the equality can be numerically evaluated based on long sequence realizations of $\boldsymbol{y}^n$ and x^n generated with respect to the distributions $P(x^n)$ and $P(\boldsymbol{y}^n|x^n)$.

3.2 Lower bound with an Auxiliary Channel Law

With the purpose to reduce the complexity of the computation of the AIR, a simplifying auxiliary channel law is used, which corresponds to a lower bound on the AIR. This section presents such a channel law for the considered CPM system as well as a method for the numerical evaluation of the lower bound on the AIR.

3.2.1 Auxiliary Channel Law

The auxiliary channel law $W(\cdot|\cdot)$ approximates the actual channel law by limiting the memory of the channel to N previous channel output symbols $\boldsymbol{y}_{k-N}^{k-1}$, i.e.,

$$P\left(\boldsymbol{y}_k|\boldsymbol{y}^{k-1},x^k\right) \approx W\left(\boldsymbol{y}_k|\boldsymbol{y}^{k-1},x^k\right) = P\left(\boldsymbol{y}_k\left|\boldsymbol{y}_{k-N}^{k-1},x^k\right.\right). \tag{3-7}$$

Employing this auxiliary channel law in (3-6), as stated in [27], the AIR can be lower bounded by

$$\begin{aligned}\overline{I}(X_k;\boldsymbol{Y}_k) &= \lim_{n\to\infty}\frac{1}{n}I(X^n;\boldsymbol{Y}^n)\\ &\geq \lim_{n\to\infty}\frac{1}{n}\left(-\log_2 W\left(\boldsymbol{y}^n\right) + \log_2 W\left(\boldsymbol{y}^n|x^n\right)\right),\end{aligned} \tag{3-8}$$

where the limit on the right hand side of (3-8) can be numerically approached with long sequences of channel output observations of the actual channel $\boldsymbol{y}^n$.

The formulation of the auxiliary channel law for the CPM system proposed in Chapter 2 is done by taking into account the channel output $\boldsymbol{y}_k$ on N previous channel realizations, $L_{\text{cpm}} + L_g + N - 1$ previous transmit

symbols and the absolute phase state, such that

$$\begin{aligned} W(\boldsymbol{y}_k|\boldsymbol{y}^{k-1}, x^n) &= P(\boldsymbol{y}_k|\boldsymbol{y}_{k-N}^{k-1}, x^n) \\ &= P(\boldsymbol{y}_k|\boldsymbol{y}_{k-N}^{k-1}, \beta_{k-L_{\text{cpm}}-L_g-N}, x_{k-L_{\text{cpm}}-L_g-N+1}^{k}) \\ &= P(\boldsymbol{y}_k|\boldsymbol{y}_{k-N}^{k-1}, \beta_{k-L}, x_{k-L+1}^{k}) \\ &= \frac{P(\boldsymbol{y}_{k-N}^{k}|\beta_{k-L}, x_{k-L+1}^{k})}{P(\boldsymbol{y}_{k-N}^{k-1}|\beta_{k-L}, x_{k-L+1}^{k-1})}, \end{aligned} \tag{3-9}$$

where $L = L_{\text{cpm}} + L_g + N$ would be the overall memory considered in the auxiliary channel law. Note that it ignores the potential dependency on further previous channel outputs $\boldsymbol{y}^{k-N-1}$, which exists because the noise samples are correlated after passing the receive filter. In order to consider the influence of the receive filter on the noise correlation and the waveform at some level, an extended state representation, namely s_k is required

$$s_k = \begin{cases} [\beta_{k-L+1}, x_{k-L+2}^{k}], & \text{if } L > 1, \\ [\beta_k], & \text{if } L = 1, \end{cases} \tag{3-10}$$

where N is brought into the model within the overall memory L. For all time index k, s_k belongs to a finite set of states, i.e.,

$$s_k \in \mathbb{S} = \{S_1, S_2, \dots S_{n_{st}}\} \tag{3-11}$$

where $n_{st} = P_{\text{cpm}} \cdot M_{\text{cpm}}^{L-1}$ is the cardinality of $\mathbb{S}$. As a consequence of this definition, the notation of the auxiliary channel law can be written in terms of the state notation s_k

$$\begin{aligned} W(\boldsymbol{y}_k|\boldsymbol{y}^{k-1}, x^n) &= P(\boldsymbol{y}_k|\boldsymbol{y}_{k-N}^{k-1}, \beta_{k-L}, x_{k-L+1}^{k}) \\ &= P(\boldsymbol{y}_k|\boldsymbol{y}_{k-N}^{k-1}, s_k, s_{k-1}). \end{aligned} \tag{3-12}$$

Note that (s_k, s_{k-1}) is equivalent to the notation $(\beta_{k-L}, x_{k-L+1}^{k})$, as the absolute phase β_{k-L+1} can be described by $(\beta_{k-L}, x_{k-L+1}^{k})$, vide equation (2-8).

3.2.2 Numerical evaluation

As illustrated in [22], the probabilities $W(\boldsymbol{y}^n)$ and $W(\boldsymbol{y}^n|x^n)$ in (3-8) can be computed recursively with the forward recursion of the Bahl-Cocke-Jelinek-Raviv (BCJR) algorithm [28]. By using the state notation s_k, $W(\boldsymbol{y}^n)$ can be

determined with the equations

$$W(\boldsymbol{y}^k) = \sum_{s_k} W(\boldsymbol{y}^k, s_k) = \sum_{s_k} \mathrm{f}_k(s_k), \tag{3-13}$$

$$\begin{aligned} \mathrm{f}_k(s_k) &= \sum_{s_{k-1}} W(\boldsymbol{y}^k, s_k, s_{k-1}) \\ &= \sum_{s_{k-1}} W\left(\boldsymbol{y}_k, s_k | \boldsymbol{y}^{k-1}, s_{k-1}\right) \cdot \mathrm{f}_{k-1}(s_{k-1}) \\ &= \sum_{s_{k-1}} P\left(\boldsymbol{y}_k | \boldsymbol{y}_{k-N}^{k-1}, s_k, s_{k-1}\right) \cdot P(s_k|s_{k-1}) \cdot \mathrm{f}_{k-1}(s_{k-1}), \end{aligned} \tag{3-14}$$

where the use of (3-12) with the forward probability $\mathrm{f}_k(s_k)$ defines the branch metric of the BCJR algorithm. Similarly the conditional probability $W(\boldsymbol{y}^n|x^n)$ is computed with the following recursion rule

$$\begin{aligned} W(\boldsymbol{y}^k|x^n) &= \tilde{\mathrm{f}}_k \\ &= W(\boldsymbol{y}_k|\boldsymbol{y}^{k-1}, x^n) \cdot W(\boldsymbol{y}^{k-1}|x^n) \\ &= P(\boldsymbol{y}_k|\boldsymbol{y}_{k-N}^{k-1}, s_k, s_{k-1}) \cdot \tilde{\mathrm{f}}_{k-1}. \end{aligned} \tag{3-15}$$

The initialization of the algorithm is performed by defining the metrics $\mathrm{f}_{k=0}(s_k)$ and $\tilde{\mathrm{f}}_{k=0} = 1$. In practice, it was observed in [27] that during the recursion steps, those branch metrics tend to go to zero after a few iterations, therefore, the recursion (3-14) is slightly changed to

$$\mathrm{f}_k(s_k) = \mu_k \sum_{s_{k-1}} P\left(\boldsymbol{y}_k | \boldsymbol{y}_{k-N}^{k-1}, s_k, s_{k-1}\right) \cdot P(s_k|s_{k-1}) \cdot \mathrm{f}_{k-1}(s_{k-1}), \tag{3-16}$$

where the scaling factors μ_k are chosen such that $\sum_{s_k} \mathrm{f}_k(s_k) = 1$. Regarding the recursion in (3-15), auxiliary variables $\tilde{\mu}_k$ are defined as

$$\tilde{\mu}_k = P(\boldsymbol{y}_k|\boldsymbol{y}_{k-N}^{k-1}, s_k, s_{k-1})^{-1},$$

with the aim of express the desired information rate quantity as

$$-\frac{1}{n}\log_2 W(\boldsymbol{y}^n) + \frac{1}{n}\log_2 W\left(\boldsymbol{y}^n|x^n\right) = \frac{1}{n}\sum_{k=1}^{n}\log_2 \mu_k - \frac{1}{n}\sum_{k=1}^{n}\log_2 \tilde{\mu}_k, \tag{3-17}$$

which approaches its true value for larges values of n.

3.3 Channel Output Probability

The Bayes' rule illustrated in (3-9), can also be rewritten in terms of the state notation s_k as follows

$$P\left(\boldsymbol{y}_k|\boldsymbol{y}_{k-N}^{k-1}, s_k, s_{k-1}\right) = \frac{P(\boldsymbol{y}_{k-N}^{k}|s_k, s_{k-1})}{P(\boldsymbol{y}_{k-N}^{k-1}|s_{k-1})}, \tag{3-18}$$

which is the probability used for the recursions in (3-14) and (3-15). Numerator and denominator in (3-18) are channel output probabilities that must be computed to serve as input to the BCJR algorithm.

According to [19], the channel output probability can be calculated for a system with CPM with 1-bit quantization by integrating the given Gaussian multivariate density distribution

$$P(\boldsymbol{y}_{k-N}^{k}|s_{k-1}, s_k) = \int\limits_{\boldsymbol{z}_{k-N}^{k} \in \mathbb{Y}_{k-N}^{k}} p(\boldsymbol{z}_{k-N}^{k-1}|s_k, s_{k-1}) d\boldsymbol{z}_{k-N}^{k}, \tag{3-19}$$

where $\mathbb{Y}_{k-N}^{k}$ represents the quantization interval which belongs to the channel output symbol $\boldsymbol{y}_{k-N}^{k}$, described in (2-14) with $\eta = N$. The vector $\boldsymbol{z}_{k-N}^{k}$ is a complex Gaussian random vector that describes the input of the ADC, with mean vector and covariance matrix defined by

$$\boldsymbol{m}_z = \boldsymbol{D}\boldsymbol{G}\left[\sqrt{\frac{E_\mathrm{s}}{T_\mathrm{s}}} e^{\psi_{k-N-L_g}^{k}}\right], \tag{3-20}$$

$$\boldsymbol{K}_z = \sigma_n^2 \boldsymbol{D}\boldsymbol{G}\boldsymbol{G}^H \boldsymbol{D}^T, \tag{3-21}$$

respectively, with $\boldsymbol{D}$ and $\boldsymbol{G}$ as introduced before in (2-12) and (2-13).

In order to numerically evaluate (3-19) using an existing quasi-Monte Carlo integration algorithm, based on methods developed in [29], a real valued formulation is required. Thus, the conditional probability density function $p(\boldsymbol{z}_{k-N}^{k}|s_k, s_{k-1})$ is written as follows

$$\begin{aligned} p(\boldsymbol{z}_{k-N}^{k}|s_k, s_{k-1}) &= \frac{1}{\sqrt{(2\pi)^{2M(N+1)}\,|\boldsymbol{K}'_z|}} \\ &\times \exp\left(-\frac{1}{2}\left(\boldsymbol{z}_{k-N}^{k\,\prime} - \boldsymbol{m}'_z\right)^T \boldsymbol{K}'^{-1}_z \left(\boldsymbol{z}_{k-N}^{k\,\prime} - \boldsymbol{m}'_z\right)\right), \end{aligned} \tag{3-22}$$

where $|\cdot|$ denotes the determinant, $\boldsymbol{z}_{k-N}^{k\,\prime} = \left[\mathrm{Re}\left\{\boldsymbol{z}_{k-N}^{k}\right\}^T, \mathrm{Im}\left\{\boldsymbol{z}_{k-N}^{k}\right\}^T\right]^T$ and the mean vector $\boldsymbol{m}'_z$ contains the real and imaginary components in a stacked

fashion as given by

$$\boldsymbol{m}'_z = \begin{bmatrix} \mathrm{Re}\{\boldsymbol{m}_z\} \\ \mathrm{Im}\{\boldsymbol{m}_z\} \end{bmatrix} = \begin{bmatrix} \mathrm{Re}\left\{ \boldsymbol{D}\ \boldsymbol{G} \begin{bmatrix} \sqrt{\frac{E_\mathrm{s}}{T_\mathrm{s}}} e^{\psi^k_{k-L_g-N}} \end{bmatrix} \right\} \\ \mathrm{Im}\left\{ \boldsymbol{D}\ \boldsymbol{G} \begin{bmatrix} \sqrt{\frac{E_\mathrm{s}}{T_\mathrm{s}}} e^{\psi^k_{k-L_g-N}} \end{bmatrix} \right\} \end{bmatrix}. \tag{3-23}$$

Accordingly, the covariance matrix is denoted as

$$\begin{aligned} \boldsymbol{K}'_z =& \mathrm{E}\left\{ \begin{bmatrix} \boldsymbol{D}\ \mathrm{Re}\{\boldsymbol{G}\} & -\boldsymbol{D}\ \mathrm{Im}\{\boldsymbol{G}\} \\ \boldsymbol{D}\ \mathrm{Im}\{\boldsymbol{G}\} & \boldsymbol{D}\ \mathrm{Re}\{\boldsymbol{G}\} \end{bmatrix} \begin{bmatrix} \mathrm{Re}\left\{\boldsymbol{n}^k_{k-L_g-N}\right\} \\ \mathrm{Im}\left\{\boldsymbol{n}^k_{k-L_g-N}\right\} \end{bmatrix} \right. \\ & \left. \times \begin{bmatrix} \mathrm{Re}\left\{\boldsymbol{n}^k_{k-L_g-N}\right\} \\ \mathrm{Im}\left\{\boldsymbol{n}^k_{k-L_g-N}\right\} \end{bmatrix}^T \begin{bmatrix} \boldsymbol{D}\ \mathrm{Re}\{\boldsymbol{G}\} & -\boldsymbol{D}\ \mathrm{Im}\{\boldsymbol{G}\} \\ \boldsymbol{D}\ \mathrm{Im}\{\boldsymbol{G}\} & \boldsymbol{D}\ \mathrm{Re}\{\boldsymbol{G}\} \end{bmatrix}^T \right\}. \end{aligned} \tag{3-24}$$

As detailed in [20], the number of evaluations n_{ev} of the multivariate integral in (3-19) required for the model, respects the proportion

$$n_{ev} \propto 4^M M^L_{\mathrm{cpm}} \tag{3-25}$$

where 4^M is the number of all possible observed complex vectors $\boldsymbol{y}_k$ and M^L_{cpm} is proportional to the number of all the possible state transitions. With this, the evaluation of all channel output probabilities becomes computationally expensive when the oversampling factor M, the modulation order M_{cpm} and the overall channel memory L are large.

3.4 Preliminary Results

This section presents preliminary results for the computation of a lower bound on the achievable rate for the discrete-time system model detailed in Section 2.5. Such results serve as a motivation for the next chapters, which propose methods to enhance the overall system performance. The results in this section were presented before in [19, 30].

3.4.1 Initial Considerations for Numerical Computations

The considered CPM signals for the results in this section have modulation order $M_{\mathrm{cpm}} = 4$ and $M_{\mathrm{cpm}} = 8$ with the modulation index $h = \frac{1}{M_{\mathrm{cpm}}}$ and no further frequency is considered with $n_{\mathrm{IF}} = 0$. The frequency pulse used for such signals is given by

$$g_f(\tau) = \frac{1}{2 \cdot T_\mathrm{s}} \mathrm{rect}\left(\frac{\tau - T_\mathrm{s}/2}{T_\mathrm{s}} \right), \tag{3-26}$$

which defines the 1REC [21] frequency pulse. To preserve the transmit waveform and its zero-crossings, a suboptimal bandpass noise filtering is considered as follows

$$g(t) = \sqrt{\frac{1}{T_g}}\text{rect}\left(\frac{t - T_\text{s}/2}{T_g}\right) \cdot e^{j2\pi\Delta f(t-T_\text{s}/2)}, \tag{3-27}$$

where $T_g = \frac{1}{2}T_\text{s}$. Such a filter is similar to the integrate and dump receiver considered in [31], but with its frequency response centered in low-IF. Note that the common receiver based on a matched filter bank is hardware demanding and not compatible with the considered 1-bit approach. Additionally the number of previous channel realizations N is chosen to be zero. In that case, for $M = 2$ the auxiliary channel is equivalent to the actual channel and for $M = 3$, noise correlation exists such that samples within one received oversampling block $\boldsymbol{y}_k$ are correlated, but there is no correlation between different blocks.

The SNR is given by the ratio between the transmit power and the product of the noise power spectral density N_0 and the two-sided 90% power containment bandwidth $B_{90\%}$

$$\text{SNR} = \frac{\lim_{T\to\infty}\frac{1}{T}\int_T |x\,(t)|^2\,dt}{N_0\ B_{90\%}} = \frac{E_\text{s}}{N_0}(T_\text{s}B_{90\%})^{-1}, \tag{3-28}$$

which alternatively can be interpreted as the ratio between the energy associated to a Nyquist interval and noise power density N_0. Note that the discrete noise samples in (2-14) have a variance of $\sigma_n^2 = N_0$. Considering that 5% out of band radiation can be tolerated at the lower and higher frequencies we get

$$\int_{-\infty}^{B_{90\%,\uparrow}} S(f)df = \int_{B_{90\%,\downarrow}}^{\infty} S(f)df = 0.95\int_{-\infty}^{\infty} S(f)df, \tag{3-29}$$

where $S(f)$ denotes the power spectral density of the complex baseband representation at zero-IF $x(t) = \sqrt{\frac{E_\text{s}}{T_\text{s}}}e^{j\phi(t)}$. With this, the power containment bandwidth is given by $B_{90\%} = B_{90\%,\uparrow} - B_{90\%,\downarrow}$.

3.4.2 Information rate results and discussion

The lower bound on the achievable rate is computed the way it is presented throughout this chapter. The Fig. 3.1 shows how oversampling increases the AIR due to the extra information provided during the symbol transitions. With $M_\text{cpm} = 4$ the achievable rate reaches $\log_2(M_\text{cpm}) = 2$ [bpcu] for higher values of SNR, on the other hand, for the low SNR regime, channel coding is in general required for practically approaching the achievable rates.

However, with $M_\text{cpm} = 8$ shown in Fig. 3.2, the achievable rate does

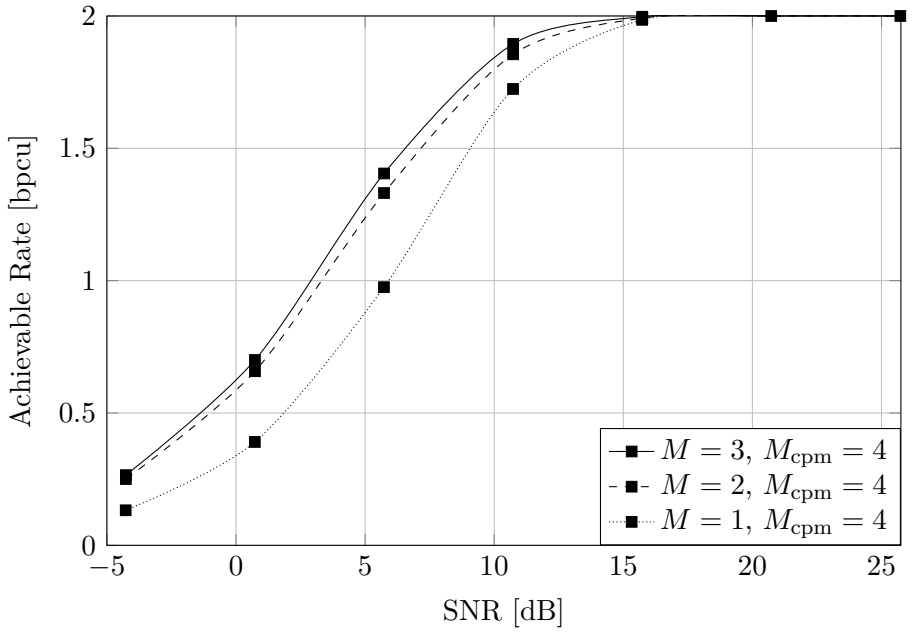

Figure 3.1: Effect of the oversampling factor M on the achievable rate for $M_{\text{cpm}} = 4$

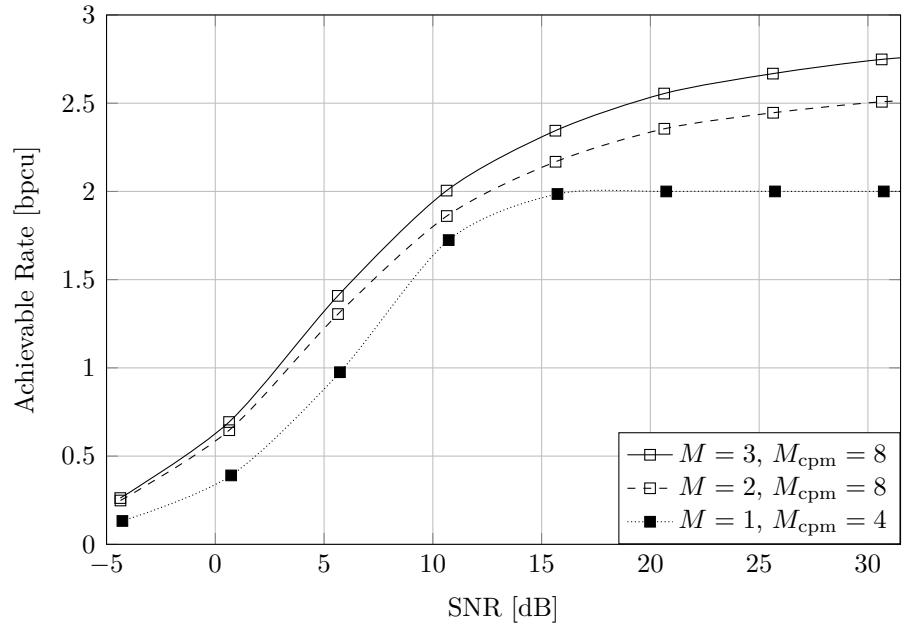

Figure 3.2: Effect of the oversampling factor M on the achievable rate for $M_{\text{cpm}} = 8$

not approach the source entropy rate of $\log_2(M_{\text{cpm}}) = 3$ [bpcu] and hence an error free transmission is impossible without channel coding. In the sequel such a channel coding scheme is studied in order to approach the addressed rates. Moreover, in the later chapters novel concepts are presented which yield higher spectral efficiency and a lower bit error rate as compared to conventional CPM signal with uniform oversampling.

4 Iterative Detection and Decoding

This chapter considers the design and analysis of CPM schemes with 1-bit quantization and oversampling at the receiver, employing convolutional codes in scenarios with higher modulation order. For such cases, e.g., $M_{\text{cpm}} = 8$, based on the achievable rates computed in the previous chapter, channel coding is essential for establishing reliable communications with low probability of error, because the achievable rate at high SNR is lower than the input entropy. In this context, it is proposed to extend the discrete system model for CPM signals received with 1-bit quantization and oversampling, presented in [19], for a sophisticated coding and decoding scheme.

For the CPM system proposed in [19, 30], with 1-bit quantization and oversampling at the receiver, the lower bound on the achievable rate is the base information used to choose or design the channel coding scheme. The parameter used to assist this choice is mainly the code rate. For a specific SNR a coding scheme must satisfy the following condition

$$0 \leq R \cdot \log_2(M_{\text{cpm}}) < I_{M_{\text{cpm}}} \leq \log_2(M_{\text{cpm}}) \text{ [bpcu]}, \tag{4-1}$$

where R denotes the code rate of the channel code and $I_{M_{\text{cpm}}}$ denotes the achievable rate conditioned on the corresponding CPM modulation scheme. Note that $\log_2(M_{\text{cpm}})$ is the maximum entropy rate of the input, which is an upper bound of the achievable rate.

4.1 Extended System Model

The system model considered in this chapter is an extension of the discrete-time system model presented in Fig. 2.6 that is proposed in [19, 30]. In this context of CPM with 1-bit quantization and oversampling at the receiver, the Fig. 4.1 illustrates the extension in terms of the additional coding blocks. The purpose of this extension is to design a system for reliable communication by considering sophisticated forward error correction.

On the transmit path, the channel encoder receives information bits and generates an encoded message adding redundant information. The encoded message is interleaved to protect the coded information against burst errors. Then, the interleaved bits are grouped according to the modulation order

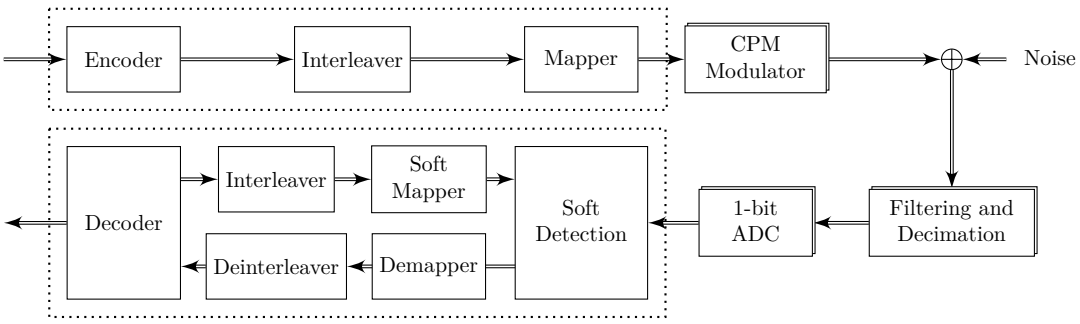

Figure 4.1: Extended discrete system model, 1-bit quantization, oversampling and coding blocks with an iterative decoding strategy

and mapped to CPM symbols. After that, a signal is generated by a CPM modulator and noise is applied due to the considered AWGN channel.

On the receive path the signal is filtered and quantized by a 1-bit ADC. The quantized data are then processed by an iterative detection and decoding (IDD) scheme. First the binary samples are processed by a soft detection algorithm. Then the soft information is converted to bit oriented log-likelihood ratios, which are deinterleaved subsequently. Finally, the soft information is given to the channel decoder, which returns extrinsic soft information to the detection algorithm via an interleaver and a soft mapper. In the sequel the individual blocks are described in detail.

4.2 Soft Detection

The maximum *a posteriori* (MAP) decision metric for each bit corresponds to the *a posteriori* probability (APP) given the received sequence $\boldsymbol{y}^n$, which, for the considered system, can be approximately computed via a BCJR algorithm [28] based on an auxiliary channel law, which is described in 3.2.1 for computing a lower bound on the achievable rate.

4.2.1 BCJR Algorithm based on an Auxiliary Channel Law

With the purpose of evaluate the APPs for the bit sequence, the value $P(s_k, s_{k-1}|\boldsymbol{y}^n)$ must be determined. This can be achieved by normalizing the joint probability $P(s_k, s_{k-1}, \boldsymbol{y}^n)$, which can be decomposed into

$$\begin{aligned} P(s_k, s_{k-1}, \boldsymbol{y}^n) &= P(s_k, s_{k-1}, \boldsymbol{y}^{k-1}, \boldsymbol{y}_k, \boldsymbol{y}_{k+1}^n) \\ &= P(s_{k-1}, \boldsymbol{y}^{k-1}) \cdot P(s_k, \boldsymbol{y}_k|\boldsymbol{y}^{k-1}, s_{k-1}) \cdot P(\boldsymbol{y}_{k+1}^n|s_k, \boldsymbol{y}^k) \\ &\approx \underbrace{W(s_{k-1}, \boldsymbol{y}^{k-1})}_{\mathrm{f}_{k-1}(s_{k-1})} \cdot \underbrace{W(s_k, \boldsymbol{y}_k|\boldsymbol{y}^{k-1}, s_{k-1})}_{\gamma_k(s_{k-1}, s_k)} \cdot \underbrace{W(\boldsymbol{y}_{k+1}^n|s_k, \boldsymbol{y}^k)}_{\mathrm{b}_k(s_k)}, \end{aligned}$$

where the considered auxiliary channel law is applied. The factor $\gamma_k(s_{k-1}, s_k)$ can be rewritten as

$$\begin{aligned}\gamma_k(s_{k-1}, s_k) &= W(s_k, \boldsymbol{y}_k|\boldsymbol{y}^{k-1}, s_{k-1}) \\ &= P(\boldsymbol{y}_k|\boldsymbol{y}_{k-N}^{k-1}, s_k, s_{k-1}) \cdot P\left(s_k|s_{k-1}\right),\end{aligned} \tag{4-2}$$

which relates to the state transition probabilities and to the channel output probability explored in section 3.3. The factor $\mathrm{f}_{k-1}(s_{k-1})$ is the forward probability which contains all the paths that leads to the state s_{k-1}. The forward recursion used to compute $\mathrm{f}_{k-1}(s_{k-1})$ is described in (3-14) and can be rewritten in terms of $\gamma_k(s_{k-1}, s_k)$

$$\begin{aligned}\mathrm{f}_k(s_k) = W(s_k, \boldsymbol{y}^k) &= \sum_{s_{k-1}} W(s_k, s_{k-1}, \boldsymbol{y}^k) \\ &= \sum_{s_{k-1}} W(s_k, \boldsymbol{y}_k|\boldsymbol{y}^{k-1}, s_{k-1}) \cdot W(s_{k-1}, \boldsymbol{y}^{k-1}) \\ &= \sum_{s_{k-1}} \gamma_k(s_{k-1}, s_k) \cdot \mathrm{f}_{k-1}(s_{k-1}).\end{aligned} \tag{4-3}$$

Finally, $\mathrm{b}_k(s_k)$ is the backward probability that contains all possible paths from state s_k to s_n. Similarly, $\mathrm{b}_k(s_k)$ is computed using the backward recursion

$$\begin{aligned}\mathrm{b}_k(s_k) = W(\boldsymbol{y}_{k+1}^n|s_k, \boldsymbol{y}^k) &= \sum_{s_{k+1}} W(s_{k+1}, \boldsymbol{y}_{k+1}^n|s_k, \boldsymbol{y}^k) \\ &= \sum_{s_{k+1}} W(s_{k+1}, \boldsymbol{y}_{k+1}|\boldsymbol{y}^k, s_k) \cdot W(\boldsymbol{y}_{k+2}^n|s_k, s_{k+1}, \boldsymbol{y}^{k+1}) \\ &= \sum_{s_{k+1}} \gamma_k(s_k, s_{k+1}) \cdot \mathrm{b}_{k+1}(s_{k+1}).\end{aligned} \tag{4-4}$$

With this, an approximate value $P_{\mathrm{aux}}(s_k, s_{k-1}|\boldsymbol{y}^n)$ of the probability $P(s_k, s_{k-1}|\boldsymbol{y}^n)$ can be computed by normalizing for $P(\boldsymbol{y}^n)$, the equation

$$P_{\mathrm{aux}}(s_k, s_{k-1}|\boldsymbol{y}^n) \cdot P(\boldsymbol{y}^n) = \mathrm{f}_{k-1}(s_{k-1}) \cdot \gamma_k(s_{k-1}, s_k) \cdot \mathrm{b}_k(s_k). \tag{4-5}$$

Note that for the recursions described in (4-3) and (4-4), initial values for $\mathrm{f}_{k=0}(s_k)$ and $\mathrm{b}_{k=n+1}(s_k)$ are required.

While the BCJR algorithm can be implemented using the steps above, it is practical to employ a matrix form of the algorithm. In order to achieve this, the following definitions are required:

- $\mathbf{f}_k$ is the vector form of the forward probabilities $\mathrm{f}_k(s_k)$ for all states at time index k;
- $\mathbf{b}_k$ is the vector form of the backward probabilities $\mathrm{b}_k(s_k)$ for all states at time index k;

- $\mathbf{\Gamma}_k(\boldsymbol{y}_{k-N}^k)$ is the matrix form of the transition probabilities $\gamma_k(s_k, s_{k+1})$ at time index k, depending on the received vector $\boldsymbol{y}_{k-N}^k$.

In more detail, the transition probability matrix $\mathbf{\Gamma}_k(\boldsymbol{y}_{k-N}^k)$ is expressed as

$$\mathbf{\Gamma}_k(\boldsymbol{y}_{k-N}^k) = \begin{bmatrix} \gamma_k(S_1, S_1) & \gamma_k(S_1, S_2) & \cdots & \gamma_k(S_1, S_{n_{st}}) \\ \gamma_k(S_2, S_1) & \gamma_k(S_2, S_2) & \cdots & \gamma_k(S_2, S_{n_{st}}) \\ \vdots & \vdots & \ddots & \vdots \\ \gamma_k(S_{n_{st}}, S_1) & \gamma_k(S_{n_{st}}, S_2) & \cdots & \gamma_k(S_{n_{st}}, S_{n_{st}}) \end{bmatrix}, \tag{4-6}$$

which allows for the matrix representation of the recursions with the equations

$$\begin{aligned} \mathbf{f}_k &= \mathbf{\Gamma}_k(\boldsymbol{y}_{k-N}^k) \cdot \mathbf{f}_{k-1} \\ \mathbf{b}_k &= \mathbf{\Gamma}_k(\boldsymbol{y}_{k-N}^k)^T \cdot \mathbf{b}_{k+1}. \end{aligned} \tag{4-7}$$

4.2.2 *A Posteriori* Probabilities and Soft Information

The probabilities $P_{\text{aux}}(s_{k-1}, s_k|\boldsymbol{y}^n)$ are used to compute the APPs for the bits that are computed by the demapper block. Letting $d^m = [d_1, \ldots, d_m]$ as the interleaved bit sequence that is mapped into CPM symbols, its bit APPs are described with the summation

$$\begin{aligned} P(d_q = d|\boldsymbol{y}^n) &= \sum_{\substack{\forall s_{k-1}, s_k \supseteq x_k \\ \text{such that} \\ \text{map}_k^{-1}(x_k, i) = d}} P_{\text{aux}}(s_k, s_{k-1}|\boldsymbol{y}^n) \\ &= \frac{1}{P(\boldsymbol{y}^n)} \sum_{\substack{\forall s_{k-1}, s_k \supseteq x_k \\ \text{such that} \\ \text{map}_k^{-1}(x_k, i) = d}} \mathrm{f}_{k-1}(s_{k-1}) \cdot \gamma_k(s_{k-1}, s_k) \cdot \mathrm{b}_k(s_k) \\ &= \frac{\mathbf{b}_k{}^T \cdot \left(\mathbf{\Sigma}_i(d) \odot \mathbf{\Gamma}_k(\boldsymbol{y}_{k-N}^k)\right) \cdot \mathbf{f}_{k-1}}{\mathbf{b}_k{}^T \cdot \mathbf{\Gamma}_k(\boldsymbol{y}_{k-N}^k) \cdot \mathbf{f}_{k-1}}, \end{aligned} \tag{4-8}$$

where $d_q = \text{map}_k^{-1}(x_k, i)$ with bit index $q = (k-1) \cdot \log_2(M_{\text{cpm}}) + i$ denotes extraction of the bit d_q, which corresponds to the i^{th} bit, most significant bit (MSB) first, of the k^{th} demapped symbol with $i \in \{1, 2, \ldots, \log_2(M_{\text{cpm}})\}$. To the vector notation in (4-8), $\mathbf{\Sigma}_i(d)$ is introduced as a matrix of 1's and 0's that translates the summation condition into an element-wise multiplication, represented by the operator $\odot$, with the matrix $\mathbf{\Gamma}_k(\boldsymbol{y}_{k-N}^k)$. More on that, the fraction $1/P(\boldsymbol{y}^n)$ is replaced by a normalization on the measurement of the probability. Finally, the whole description of the soft detection algorithm is described in Table 4.1.

The posterior probabilities $P(d_q|\boldsymbol{y}^n)$ are the natural choice for the soft

Input

– Received sequence $\boldsymbol{y}^n$
– Transition probabilities $\boldsymbol{\Gamma}_k(\boldsymbol{y}_{k-N}^k)$
– Summation matrix $\boldsymbol{\Sigma}_i(d)$ depending on the bit mapping of symbols

Initialization

$\mathbf{f}_0 = \mathbf{1}_{n_{st}}/n_{st}$
$\mathbf{b}_{n+1} = \mathbf{1}_{n_{st}}/n_{st}$

BCJR Algorithm

for $k = 1$ **to** n **do**
  $\mathbf{f}_k = \boldsymbol{\Gamma}_k(\boldsymbol{y}_{k-N}^k) \cdot \mathbf{f}_{k-1}$ ▷ forward recursion
  $\mathbf{f}_k = \mathbf{f}_k/(\mathbf{f}_k^T \cdot \mathbf{1}_{n_{st}})$ ▷ normalization
end for

for $k = n$ **to** 1 **do**
  $\mathbf{b}_k = \boldsymbol{\Gamma}_k(\boldsymbol{y}_{k-N}^k)^T \cdot \mathbf{b}_{k+1}$ ▷ backward recursion
  $\mathbf{b}_k = \mathbf{b}_k/(\mathbf{b}_k^T \cdot \mathbf{1}_{n_{st}})$ ▷ normalization
end for

Output

$$P(d_q = d|\boldsymbol{y}^n) = {\mathbf{b}_k}^T \cdot \left(\boldsymbol{\Sigma}_i(d) \odot \boldsymbol{\Gamma}_k(\boldsymbol{y}_{k-N}^k)\right) \cdot \mathbf{f}_{k-1} / {\mathbf{b}_k}^T \cdot \boldsymbol{\Gamma}_k(\boldsymbol{y}_{k-N}^k) \cdot \mathbf{f}_{k-1}$$

Table 4.1: Soft Detection with BCJR Algorithm

information $\mathfrak{s}(d_q)$ about the demapped bits. Such probabilites can also be expressed by marginalizing over d_q in the sequence-base posterior probability $P(d^m|\boldsymbol{y}^n)$, where $m = n \cdot \log_2(M_{\text{cpm}})$, with the following expressions

$$\begin{aligned} P(d_q = d|\boldsymbol{y}^n) &= \sum_{d^m|d_q=d} P(d^m|\boldsymbol{y}^n) \\ &= \frac{1}{P(\boldsymbol{y}^n)} \sum_{d^m|d_q=d} P(\boldsymbol{y}^n|d^m) \cdot P(d^m). \end{aligned} \tag{4-9}$$

With binary random variables described by the probabilities $P(d_q = 0|\boldsymbol{y}^n)$ and $P(d_q = 1|\boldsymbol{y}^n)$, the use of log-likelihood ratios (LLR) given the received sequence $\boldsymbol{y}^n$ is appropriate [32] and obtained with

$$L(d_q|\boldsymbol{y}^n) = \ln \frac{P(d_q = 0|\boldsymbol{y}^n)}{P(d_q = 1|\boldsymbol{y}^n)} = \ln \frac{\mathfrak{s}(d_q = 0)}{\mathfrak{s}(d_q = 1)}, \tag{4-10}$$

which can be decomposed, according to [32, 33], into an extrinsic and an a

priori LLR as follows

$$\begin{aligned} L(d_q|\boldsymbol{y}^n) &= \ln \frac{\sum_{d^m|d_q=0} P(\boldsymbol{y}^n|d^m) \cdot P(d^m)}{\sum_{d^m|b_q=1} P(\boldsymbol{y}^n|d^m) \cdot P(d^m)} \\ &= \ln \frac{\sum_{d^m|d_q=0} P(\boldsymbol{y}^n|d^m) \cdot \prod_{j=1;j\neq q}^{m} P(d_j)}{\sum_{d^m|d_q=1} P(\boldsymbol{y}^n|d^m) \cdot \prod_{j=1;j\neq q}^{m} P(d_j)} + \ln \frac{P(c_q=0)}{P(d_q=1)} \\ &= L_{\text{ext}}(d_q|\boldsymbol{y}^n) + \ln \frac{P(d_q=0)}{P(d_q=1)} \\ &= L_{\text{ext}}(d_q|\boldsymbol{y}^n) + L(d_q). \end{aligned} \tag{4-11}$$

The extrinsic LLR $L_{\text{ext}}(d_q|\boldsymbol{y}^n)$ represents the information about d_q contained in $\boldsymbol{y}^n$ and $P(d_j)$ for all $j \neq q$. The *a priori* LLR $L(d_q)$ describes the available *a priori* information about d_q. The concept of extrinsic information is a crucial point in the context of turbo equalization, which will be explained in detail in the next section.

4.3 Channel Coding and Iterative Decoding

The iterative decoding process relies on the feedback of soft information from the decoder to adjust the transition probabilities of the soft detector, which becomes aware of the underlying code. Let $c^m = [c_1, \ldots, c_m]$ the code bit sequence that represents the encoded message. The soft information $\mathfrak{s}(c_q)$, with $q \in \{1, \ldots, m\}$, serves as the input of the channel decoder, which computes an update version $\mathfrak{s}'(c_q)$ of this soft information, which reads as

$$\mathfrak{s}'(c_q) = P(c_q|\mathfrak{s}(c_1), \mathfrak{s}(c_2), \ldots, \mathfrak{s}(c_m)). \tag{4-12}$$

The redundancy introduced during the encoding process certifies that the reliability of $\mathfrak{s}'(c_q)$ is generally improved by the channel decoder in comparison to $\mathfrak{s}(c_q)$. This soft information is interleaved into the sequence corresponded to $\mathfrak{s}'(d_q)$, which is incorporated to the soft detector, that uses this knowledge acquired from the channel decoder to recompute $\mathfrak{s}(d_q)$. This message passing algorithm is done iteratively with soft information exchange between the detection and decoding steps. Following the described steps, the bit error rate can be improved in comparison to the scenario without feedback information. However, even better results in terms of bit error rate can be achieved when the following information is fed back from the decoder to the detector:

$$\mathfrak{s}'_{\text{ext}}(c_q) = P(c_q|\mathfrak{s}(c_1), \ldots, \mathfrak{s}(c_{q-1}), \mathfrak{s}(c_{q+1}), \ldots, \mathfrak{s}(c_m)), \tag{4-13}$$

which is the extrinsic soft information about c_q contained in $\mathfrak{s}(c_1), \ldots, \mathfrak{s}(c_m)$ except of $\mathfrak{s}(c_q)$. The idea of passing extrinsic soft information between the receive algorithms was first proposed in [33] for decoding turbo codes and has been applied to coded data transmission over channels with intersymbol interference (ISI) [34, 35], where it is called turbo equalization. In practical terms, it is often more convenient to replace the two probabilities $\mathfrak{s}(d_q = 0)$ and $\mathfrak{s}(d_q = 1)$ by the LLR in (4-10), which reads as

$$\lambda(d_q) = L(d_q|\boldsymbol{y}^n) = \ln \frac{\mathfrak{s}(d_q = 0)}{\mathfrak{s}(d_q = 1)}.$$

Accordingly, instead of the extrinsic soft information $\mathfrak{s}'_{\text{ext}}(c_q)$, the extrinsic LLR is considered, which can be expressed with

$$\lambda'_{\text{ext}}(c_q) = \ln \frac{\mathfrak{s}'_{\text{ext}}(c_q = 0)}{\mathfrak{s}'_{\text{ext}}(c_q = 1)} = \frac{P(c_q = 0|\mathfrak{s}(c_1), \ldots, \mathfrak{s}(c_{q-1}), \mathfrak{s}(c_{q+1}), \ldots, \mathfrak{s}(c_m))}{P(c_q = 1|\mathfrak{s}(c_1), \ldots, \mathfrak{s}(c_{q-1}), \mathfrak{s}(c_{q+1}), \ldots, \mathfrak{s}(c_m))}.$$

Because $\mathfrak{s}'(c_q)$ is a posterior probability, a decomposition similar to (4-11), can be applied with $\lambda'(c_q)$, which yields

$$\begin{aligned}\lambda'_{\text{ext}}(c_q) &= \frac{P(c_q = 0|\mathfrak{s}(c_1), \ldots, \mathfrak{s}(c_m))}{P(c_q = 1|\mathfrak{s}(c_1), \ldots, \mathfrak{s}(c_m))} - \ln \frac{\mathfrak{s}(c_q = 0)}{\mathfrak{s}(c_q = 1)} \\ &= \ln \frac{\mathfrak{s}'(c_q = 0)}{\mathfrak{s}'(c_q = 1)} - \ln \frac{\mathfrak{s}(c_q = 0)}{\mathfrak{s}(c_q = 1)} \\ &= \lambda'(c_q) - \lambda(c_q). \end{aligned} \tag{4-14}$$

The iterative decoding steps are summarized in Fig. 4.2, were the soft information exchange between detector and decoder is represented with the considered LLRs. In the sequel, more details on the turbo equalization method are discussed.

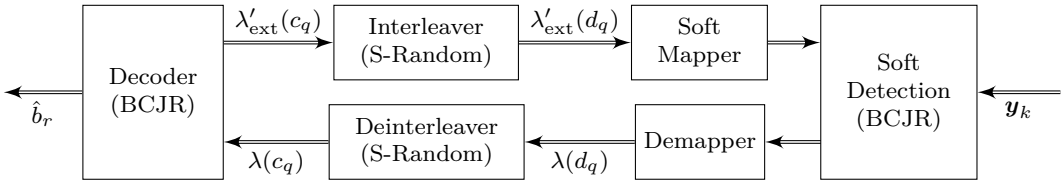

Figure 4.2: Iterative Decoding procedure on receive path of the system model

4.3.1 Interleaving and Deinterleaving

The interleaving process shuffles the bits according to a permutation function, say $\Pi(\cdot)$, on the bit indexes, i.e., $\Pi : \{1, \ldots, m\} \to \{1, \ldots, m\}$. During

the transmit path the code bits are interleaved given such a permutation, expressed as

$$[c_1, \ldots, c_m] \xrightarrow{interleaving} [d_1, \ldots, d_m],$$

where $c_q = d_{\Pi(q)}$. Regarding the receive path, the detection algorithm outputs the demapped bit-related LLR sequence, which is deinterleaved according to the considered permutation, as follows

$$[\lambda(d_1), \ldots, \lambda(d_m)] \xrightarrow{deinterleaving} [\lambda(c_1), \ldots, \lambda(c_m)],$$

such that $\lambda(d_{\Pi(q)}) = \lambda(c_q)$. The resulting sequence represents the detected soft information used as input for the channel decoder.

With an iterative decoding scheme the interleaving operation happens not only in the transmit path, but also in the receive path, as follows

$$[\lambda'_{\text{ext}}(c_1), \ldots, \lambda'_{\text{ext}}(c_m)] \xrightarrow{interleaving} [\lambda'_{\text{ext}}(d_1), \ldots, \lambda'_{\text{ext}}(d_m)],$$

where extrinsic soft information about the code bits are routed to the soft detection processing from the channel decoder.

4.3.2 Convolutional Codes

This chapter uses convolutional codes as the simplest non-trivial example for channel coding. Convolutional codes are characterized by their constraint length and its generator polynomials [36], often represented in its octal form, e.g., (5 7). In general, a longer constraint length code has better performance in terms of bit error rate, but it requires more computation resources in the decoder. The Fig. 4.3 represents a convolutional encoder that takes one input bit and outputs two coded bits, meaning that its code rate is 1/2.

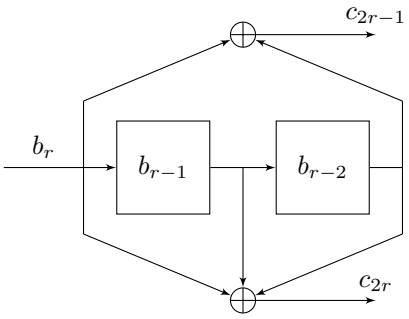

Figure 4.3: Example of Convolutional Encoder (5 7) with code rate 1/2

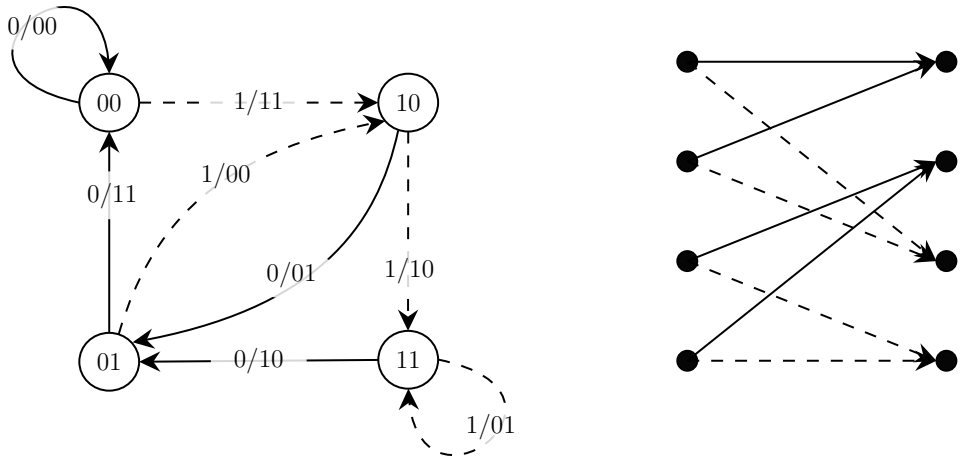

Figure 4.4: Example of Convolutional Encoder from Fig. 4.3 represented as a state machine (left) and as a trellis (right)

The convolutional codes can also be described by a state machine. The state is basically the status of the shift registers values. From that a trellis structure can be derived, which is the base description of the code used in the decoding process, that can be implemented using the Viterbi algorithm, which is a maximum likelihood (ML) decoder, or using the BCJR algorithm (MAP decoder). For instance, the formulation of a soft-input soft-output (SISO) channel decoder that takes into account the encoder illustrated in Fig. 4.3 and Fig. 4.4 can be described by the algorithm presented in Table 4.2.

High rate convolutional codes, e.g., 3/4, can be implemented using the puncturing technique to create any desired code rate from a basic low-rate code [37]. This is used to adapt the code rate while keeping a low-complexity decoder. Puncturing can be applied to modify the system throughput and robustness level by changing the puncturing pattern, which describes the bits that are propagated and discarded during the encoding procedure. The decoder must take this pattern into account to compute metrics and survivor paths. For a SISO decoder, e.g., the one considered in the Table 4.2, the corresponding discarded bits of the pattern are inserted into the LLR sequence as a zero valued LLR, so no information about the discarded bit exists on the receive path.

4.3.3 Turbo Equalization

The turbo equalization described in [35] guided the iterative decoding procedure implemented for results contained in this chapter. This iterative decoding consists of the exchange of soft information between the detector and the channel decoder. This scenario is illustrated in Fig. 4.2.

Input

$$\boldsymbol{\Gamma}_r = \begin{bmatrix} \mathfrak{s}(c_{2r-1}=0)\mathfrak{s}(c_{2r}=0) & \mathfrak{s}(c_{2r-1}=1)\mathfrak{s}(c_{2r}=1) & 0 & 0 \\ 0 & 0 & \mathfrak{s}(c_{2r-1}=0)\mathfrak{s}(c_{2r}=1) & \mathfrak{s}(c_{2r-1}=1)\mathfrak{s}(c_{2r}=0) \\ \mathfrak{s}(c_{2r-1}=1)\mathfrak{s}(c_{2r}=1) & \mathfrak{s}(c_{2r-1}=0)\mathfrak{s}(c_{2r}=0) & 0 & 0 \\ 0 & 0 & \mathfrak{s}(c_{2r-1}=1)\mathfrak{s}(c_{2r}=0) & \mathfrak{s}(c_{2r-1}=0)\mathfrak{s}(c_{2r}=1) \end{bmatrix}$$

for $r = 1, 2, 3, \ldots, m/2$

$$\boldsymbol{U}(0) = \begin{bmatrix} 1 & 1 & 0 & 0 \\ 0 & 0 & 1 & 1 \\ 0 & 0 & 0 & 0 \\ 0 & 0 & 0 & 0 \end{bmatrix}, \boldsymbol{U}(1) = \begin{bmatrix} 0 & 0 & 0 & 0 \\ 0 & 0 & 0 & 0 \\ 1 & 1 & 0 & 0 \\ 0 & 0 & 1 & 1 \end{bmatrix}$$

Initialization

$\mathbf{f}_0 = [1\ 0\ 0\ 0]^T$
$\mathbf{b}_{m/2+1} = [1\ 0\ 0\ 0]^T$

BCJR Algorithm

for $r = 1$ **to** $m/2$ **do**
  $\mathbf{f}_r = \Gamma_r \cdot \mathbf{f}_{r-1}$ ▷ forward recursion
  $\mathbf{f}_r = \mathbf{f}_r / (\mathbf{f}_r^T \cdot \mathbf{1}_4)$ ▷ normalization
end for

for $r = m/2$ **to** 1 **do**
  $\mathbf{b}_r = \Gamma_r^T \cdot \mathbf{b}_{r+1}$ ▷ backward recursion
  $\mathbf{b}_r = \mathbf{b}_r / (\mathbf{b}_r^T \cdot \mathbf{1}_4)$ ▷ normalization
end for

Output

$$P(b_r = b|\mathfrak{s}(c_1), \mathfrak{s}(c_2), \ldots, \mathfrak{s}(c_m)) = \mathbf{b}_r{}^T \cdot (\boldsymbol{U}(b) \odot \boldsymbol{\Gamma}_r) \cdot \mathbf{f}_{r-1} / (\mathbf{b}_r{}^T \cdot \boldsymbol{\Gamma}_r \cdot \mathbf{f}_{r-1})$$

Table 4.2: Channel Decoder with BCJR Algorithm

Initially, the state transition probabilities are considered to be uniformly distributed, i.e., $P(s_k|s_{k-1}) = 1/M_{\text{cpm}}$, such assumption is suboptimal, but it is possible to take into account that state transitions can have different probabilities by feeding back updated extrinsic soft information about the code bits. This extrinsic information, can be computed during the channel decoding procedure by means of employing a second BCJR algorithm. For instance, the channel decoder described in Table 4.2 for a memory-2 convolutional code illustrated in Fig. 4.3, can output the soft information in (4-12) with

$$\begin{aligned} \mathfrak{s}'(c_{2r-1}) &= P(c_{2r-1} = c|\mathfrak{s}(c_1), \mathfrak{s}(c_2), \ldots, \mathfrak{s}(c_m)) \\ &= \mathbf{b}_r{}^T \cdot (\boldsymbol{V}_{-1}(c) \odot \boldsymbol{\Gamma}_r) \cdot \mathbf{f}_{r-1} / (\mathbf{b}_r{}^T \cdot \boldsymbol{\Gamma}_r \cdot \mathbf{f}_{r-1}), \end{aligned} \tag{4-15}$$

$$\begin{aligned} \mathfrak{s}'(c_{2r}) &= P(c_{2r} = c|\mathfrak{s}(c_1), \mathfrak{s}(c_2), \ldots, \mathfrak{s}(c_m)) \\ &= \mathbf{b}_r{}^T \cdot (\boldsymbol{V}_0(c) \odot \boldsymbol{\Gamma}_r) \cdot \mathbf{f}_{r-1} / (\mathbf{b}_r{}^T \cdot \boldsymbol{\Gamma}_r \cdot \mathbf{f}_{r-1}), \end{aligned} \tag{4-16}$$

where

$$\boldsymbol{V}_{-1}(0) = \begin{bmatrix} 1 & 0 & 0 & 0 \\ 0 & 0 & 1 & 0 \\ 0 & 1 & 0 & 0 \\ 0 & 0 & 0 & 1 \end{bmatrix}, \quad \boldsymbol{V}_{-1}(1) = \begin{bmatrix} 0 & 1 & 0 & 0 \\ 0 & 0 & 0 & 1 \\ 1 & 0 & 0 & 0 \\ 0 & 0 & 1 & 0 \end{bmatrix},$$

$$\boldsymbol{V}_{0}(0) = \begin{bmatrix} 1 & 0 & 0 & 0 \\ 0 & 0 & 0 & 1 \\ 0 & 1 & 0 & 0 \\ 0 & 0 & 1 & 0 \end{bmatrix}, \quad \boldsymbol{V}_{0}(1) = \begin{bmatrix} 0 & 1 & 0 & 0 \\ 0 & 0 & 1 & 0 \\ 1 & 0 & 0 & 0 \\ 0 & 0 & 1 & 1 \end{bmatrix}.$$

With this, it is possible to compute the extrinsic LLR described in (4-14) with the following expression

$$\lambda'_{\text{ext}}(c_{2r+i}) = \ln \frac{\mathbf{b}_r{}^T \cdot (\boldsymbol{V}_i(0) \odot \boldsymbol{\Gamma}_r) \cdot \mathbf{f}_{r-1}}{\mathbf{b}_r{}^T \cdot (\boldsymbol{V}_i(1) \odot \boldsymbol{\Gamma}_r) \cdot \mathbf{f}_{r-1}} - \lambda(c_{2r+i}),$$

where $i \in \{-1, 0\}$. As asserted in [35], this equation faces problems when a numerical evaluation is performed due to the logarithm nature of the difference on the right-hand side (RHS) of the equality. To solve this for practical implementations, $\lambda'_{\text{ext}}(c_q)$ is computed as follows:

$$\lambda'_{\text{ext}}(c_{2r+i}) = \ln \frac{\mathbf{b}_r{}^T \cdot (\boldsymbol{V}_i(0) \odot \boldsymbol{\Gamma}_{\text{ext},i,r}) \cdot \mathbf{f}_{r-1}}{\mathbf{b}_r{}^T \cdot (\boldsymbol{V}_i(1) \odot \boldsymbol{\Gamma}_{\text{ext},i,r}) \cdot \mathbf{f}_{r-1}}, \tag{4-17}$$

where $\boldsymbol{\Gamma}_{\text{ext},i,r}$ are extrinsic transition matrices, that has the dependency on the input LLR $\lambda(c_{2r+i})$ removed, while computing $\lambda'_{\text{ext}}(c_{2r+i})$. For example, the extrinsic transition matrix $\boldsymbol{\Gamma}_{\text{ext},-1,r}$ corresponding to $\lambda'_{\text{ext}}(c_{2r-1})$, for the convolutional code that has been considered so far, is given by

$$\boldsymbol{\Gamma}_{\text{ext},-1,r} = \begin{bmatrix} \mathfrak{s}(c_{2r}=0) & \mathfrak{s}(c_{2r}=1) & 0 & 0 \\ 0 & 0 & \mathfrak{s}(c_{2r}=1) & \mathfrak{s}(c_{2r}=0) \\ \mathfrak{s}(c_{2r}=1) & \mathfrak{s}(c_{2r}=0) & 0 & 0 \\ 0 & 0 & \mathfrak{s}(c_{2r}=0) & \mathfrak{s}(c_{2r}=1) \end{bmatrix}.$$

The extrinsic LLRs computed with (4-17) are interleaved into a sequence represented by the soft information $\lambda'_{\text{ext}}(d_q)$ and soft mapped to new values of state transition probabilities $P(s_k|s_{k-1})$. This soft mapping is achieved by bringing the log-likelihood representation back to a probability description [35],

which is given by

$$\begin{aligned} P(s_k|s_{k-1}) &= P(x_k) \\ &= \prod_{i=1}^{\log_2(M_{\text{cpm}})} \frac{\exp\left(-b'_i \cdot \lambda'_{\text{ext}}(d_q)\right)}{1+\exp\left(-\lambda'_{\text{ext}}(d_q)\right)}\Bigg|_{q=(k-1)\cdot\log_2(M_{\text{cpm}})+i}, \\ x_k &= \text{map}([b'_1,\ldots,b'_{\log_2(M_{\text{cpm}})}]), \end{aligned} \tag{4-18}$$

where x_k is the input symbol that produce the state transition from the state s_{k-1} to s_k, $[b'_1,\ldots,b'_{\log_2(M_{\text{cpm}})}]$ is the bit sequence which such symbol is mapped to, and $\lambda'_{\text{ext}}(d_q)$ represents the interleaved extrinsic soft information fed back by the channel decoder of the bit d_q. The probabilities $P\left(s_k|s_{k-1}\right)$ can be used to perform the soft detection step again by updating the transition probabilities in the BCJR algorithm, detailed in 4.2.1.

In the final step of the channel decoder, i.e., after the execution of the required number of iterations, the soft information on the information bits are computed

$$\lambda(b_r) = \ln \frac{P(b_r=0|\mathfrak{s}(c_1),\ldots,\mathfrak{s}(c_m))}{P(b_r=1|\mathfrak{s}(c_1),\ldots,\mathfrak{s}(c_m))}, \quad \forall r \in \{1,\ldots,m\cdot R\}, \tag{4-19}$$

where R is the used code rate. At last, the estimation of the original information bits are evaluated based on the sign of the corresponding soft information $\lambda(b_r)$

$$\hat{b}_r = \begin{cases} 1, & \text{if } \lambda(b_r) < 0, \\ 0, & \text{if } \lambda(b_r) \geq 0, \end{cases} \tag{4-20}$$

To summarize this section, the iterative decoding steps illustrated in Fig. 4.2 is described in Table 4.3.

4.4 Proposed Modified Sub-channel Coding

The extra amount of information provided by the oversampling is often not enough for the system to provide reliable communication, which motivated the proposition of the CPM system in Fig. 4.1 with additional coding blocks. With the purpose to further improve the performance of the proposed system, this section covers a different coding strategy and an alternative bit mapping scheme illustrated for the example of $M_{\text{cpm}} = 8$.

4.4.1 Bit Mapping

For the considered CPM waveform with $L_{\text{cpm}} = 1$, the 1-bit quantization of the in-phase and quadrature components leads to a four-level phase decision,

Iterative Detection and Decoding	
(1)	**Initialization:** Set $P(s_k\|s_{k-1}) = 1/M_{\text{cpm}}$ for every possible state transition, to evaluate the transition probabilities $\gamma_k(s_{k-1}, s_k)$ in (4-2)
(2)	**Soft Detection and Demapping:** Perform the BCJR Algorithm described in Subsection 4.2.1, compute the *A Posteriori* Probabilities in (4-8) based on the adopted bit mapping, and evaluate the LLR sequence corresponding to $\lambda(d_q)$ for all $q \in \{1, \ldots, m\}$
(3)	**Deinterleaving:** Permute the LLR sequence $[\lambda(d_1), \ldots, \lambda(d_m)]$ into $[\lambda(c_1), \ldots, \lambda(c_m)]$
(4)	**Soft Decoding:** Use the SISO decoder to compute the soft information $\lambda(b_r)$ and feed back the extrinsic soft information $\lambda'_{\text{ext}}(c_q)$ for all $q \in \{1, \ldots, m\}$
(5)	**Termination:** verify the stop condition, i.e., whether the number of iterations has been achieved. If so, the bit estimations $\hat{b}_r$ are computed for all $r \in \{1, \ldots, m \cdot R\}$, vide (4-20)
(6)	**Interleaving:** Permute the extrinsic soft information sequence $[\lambda'_{\text{ext}}(c_1), \ldots, \lambda'_{\text{ext}}(c_m)]$ into $[\lambda'_{\text{ext}}(d_1), \ldots, \lambda'_{\text{ext}}(d_m)]$
(7)	**Soft Mapping:** compute new values of $P(s_k\|s_{k-1})$ based on the soft mapping in (4-18) and update values for $\gamma_k(s_{k-1}, s_k)$
(8)	go to (2)

Table 4.3: Iterative detection and decoding algorithm steps

which grants two bits of information when the sample at time $\tau = T_s$ is observed in a noise free scenario. This is the reason why, when noise is considered, the computed achievable rate for $M_{\text{cpm}} = 4$ reaches 2 bpcu in a high SNR regime, vide Fig. 3.1. As it was concluded from Chapter 3, more than two bits per channel use can be achieved with oversampling, which allows for the extraction of more information along the phase transition between the phase states. This is shown in Fig. 3.2 with the achievable rate result for $M_{\text{cpm}} = 8$. This idea is key to understand the motivation to study bit mapping alternatives, and how the available information at the receiver is distributed for the bits. In summary, this subsection presents two mapping strategies and how they deal with bit allocation.

The Fig. 4.5 shows the CPM tilted phase constellation on how bit sets are associated to the phase transition when using the Gray mapping, given an "even" or an "odd" initial state, whose parity is defined by the parity of the absolute phase state described in (2-8). The symbols are distinguished by on how much the phase is increased for each possible input.

The established Gray mapping scheme implies well known benefits for conventional communication systems. However, in the sequel it is proposed to modify the Gray coding scheme in order to enable the exploitation of the properties of the CPM system with 1-bit quantization and oversampling at the receiver. Similarly to the Gray mapping the Fig. 4.6 illustrates the CPM

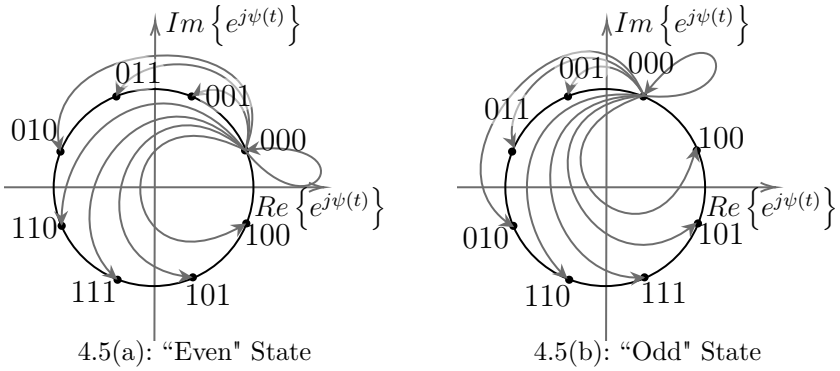

4.5(a): “Even" State 4.5(b): “Odd" State

Figure 4.5: Gray Mapping for 8-CPFSK with 1-bit quantization

tilted phase transitions with the corresponding bits for the novel mapping scheme, termed advanced mapping, which allows for the separation of the information that can be readily extracted from the orthants of the symbols and the additional information brought by oversampling. In this regard, it is possible to divide the $\log_2(M_{\text{cpm}}) = 3$ bits into binary sub-channels where two sub-channels can each yield up to 1 bit per channel use and the third sub-channel yields a lower achievable rate which depends on the oversampling factor.

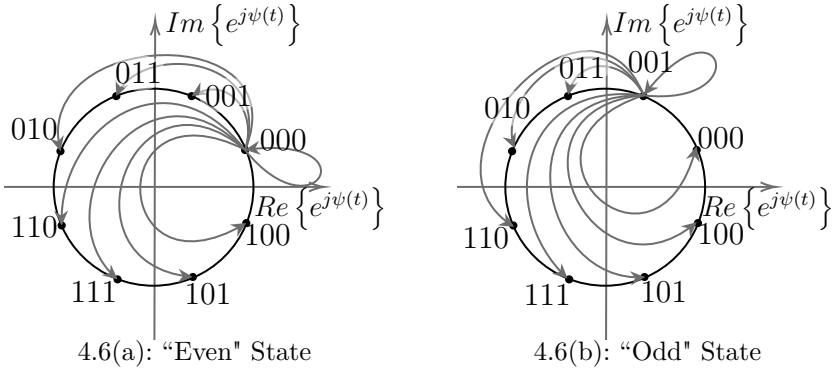

4.6(a): “Even" State 4.6(b): “Odd" State

Figure 4.6: Advanced Mapping for 8-CPFSK with 1-bit quantization

The gray mapping shuffles the uncertainties brought by the coarse quantization for every bit sub-channel, whereas the advanced mapping aims to concentrate the uncertainty on the third bit, by doing a circular shift on the gray mapping when phase transition happens from a phase state of “odd" order. The Fig. 4.7(b) proves what is being said by showing increased BER performance on the first two bits of the mapping in comparison with Fig. 4.7(a).

4.4.2 Sub-channel Coding Scheme

The coding scheme which is referred as the conventional approach, consists of the system model illustrated in Fig. 4.1, that contemplates the

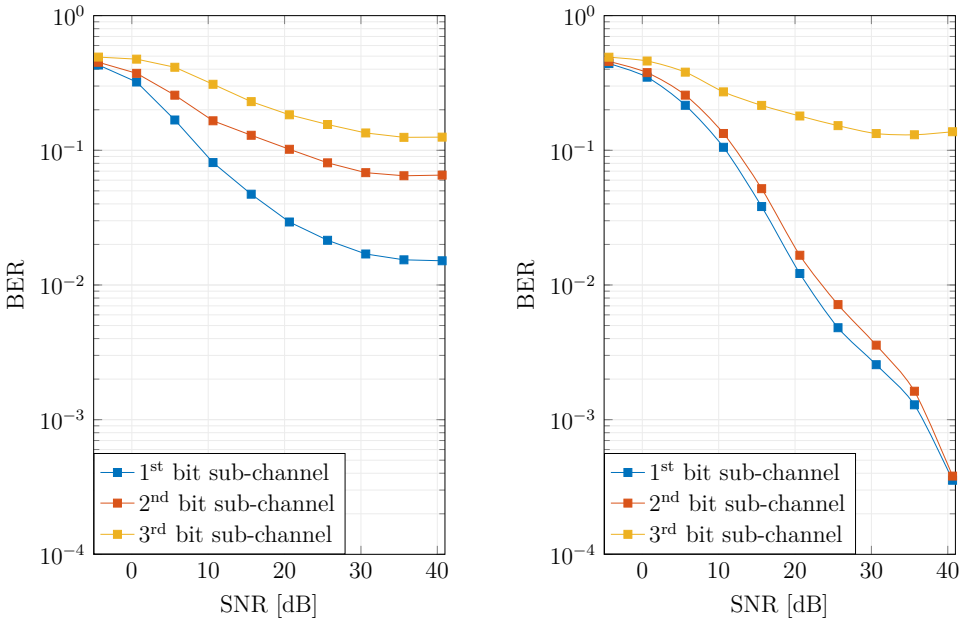

4.7(a): Gray Mapping

4.7(b): Advanced Mapping

Figure 4.7: BER results for each bit sub-channels according to the considered bit mapping, $M = 3$

use of channel coding for forward error correction (FEC), interleavers to protect the system against burst errors and an iterative decoding procedure as part of a sophisticated channel decoding approach. However, no regard with respect to bit sub-channel performance, presented in Fig. 4.7, is taken into account. In order to take advantage of the novel advanced mapping, a modified coding scheme is proposed. This coding scheme has the same structure of the conventional one, but applies different code rates for the bit sub-channels separately, i.e., in transmission, bit sub-channels streams that are more sensitive to noise or channel impairments would pass through a channel encoder with a lower code rate.

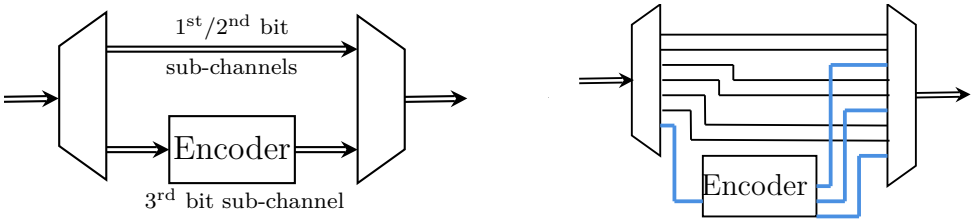

4.8(a): Coding Scheme

4.8(b): Scheme for $R = 7/9$

Figure 4.8: Proposed Coding Scheme for $M_{\text{cpm}} = 8$

For the case study, no coding is applied to the first two bit sub-channels whereas a strong convolutional code is applied to the third sub-channel. This

is illustrated in Fig. 4.8(a), where in (b) a code rate of 1/3 is applied to the third sub-channel, which corresponds to an overall code rate of $R = 7/9$.

4.5 Bit Error Rate Results and discussion

All the computations rely on $M_{\text{cpm}} = 8$, modulation index $h = \frac{1}{M_{\text{cpm}}}$ and oversampling factor $M = 3$. The simulation environment is set in a similar fashion to what is considered in Section 3.4.1. For instance, the used frequency pulse is the 1REC in (3-26) and the receive filter is assumed to be the suboptimal bandpass filter in (3-27). Additionally, the SNR definition is brought from equation (3-28) and reads as

$$\text{SNR} = \frac{E_{\text{s}}}{N_0}(T_{\text{s}}B_{90\%})^{-1},$$

where $B_{90\%}$ denotes the 90% power containment bandwidth. With respect to channel decoding parameters used in this section, the Table 4.4 displays puncturing patterns applied to convolutional codes represented by their polynomial generator in its octal form. For the simulations in this section, blocks containing approximately 1000 information bits are randomly generated to be input of the CPM system.

Code Rate	Generator	Puncturing Pattern
1/3	(5 7 7)	1 1 1
1/2	(5 7)	1 1
2/3	(5 7)	1 1 | 0 1
3/4	(5 7)	1 1 | 0 1 | 1 0

Table 4.4: Puncturing patterns examples for codes with constraint length $K_{cc} = 3$

Bit error rate results are presented as the comparative performance evaluation of the methods and ideas described in this chapter.

4.5.1 Number of iterations

Given the presented scenario applied to the extended system model described in Fig. 4.1, it is possible to observe the gain provided by the iterative decoding scheme by varying the number of iterations parameter. From the Fig. 4.9, one is able to notice that after the second iteration, the iterative process grants a decreased BER performance gain. Naturally, the simulation results show that using channel coding with lower code rates yield a better BER performance.

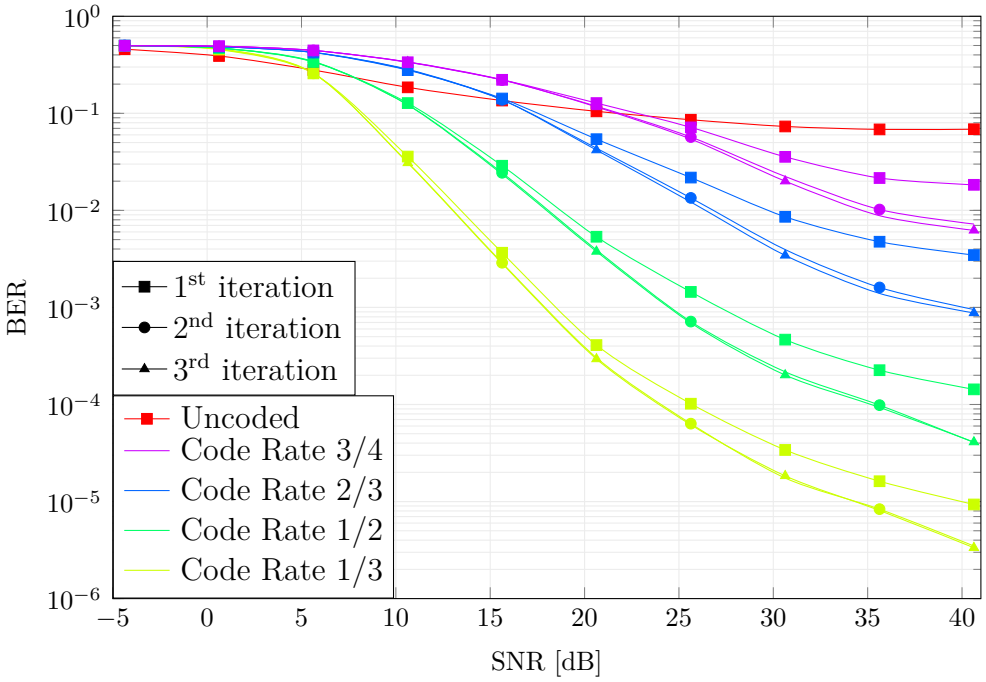

Figure 4.9: BER results for the considered CPM signal with channel coding of different code rates and constraint length $K_{cc} = 3$ using Gray Mapping

4.5.2 Novel bit mapping

The bit mapping is the first part of the proposed enhancements presented in Section 4.4 to be analyzed. The Gray mapping is compared against the novel advanced mapping. The Fig. 4.10 illustrates the BER simulation results, which confirm that system designs using Advanced mapping outperform system designs using Gray mapping in terms of BER. For systems with Gray mapping three iterations are considered and for systems with Advanced mapping only two, because no further performance gain was observed by increasing the iterations for the latter.

4.5.3 Sub-channel coding

Finally, in Fig. 4.11, the BER results for the proposed coding scheme are presented. The conventional coding scheme uses a convolutional code with rate 7/9, generator polynomial (5 7) and puncturing pattern 11|01|01|10|10|01|11. In contrast, the proposed coding scheme uses a convolutional code with rate 1/3 for the third bit sub-channel as shown in Fig. 4.8(b). In this last scenario, the use of the proposed coding scheme brings a consistent performance gain from low to high SNR levels.

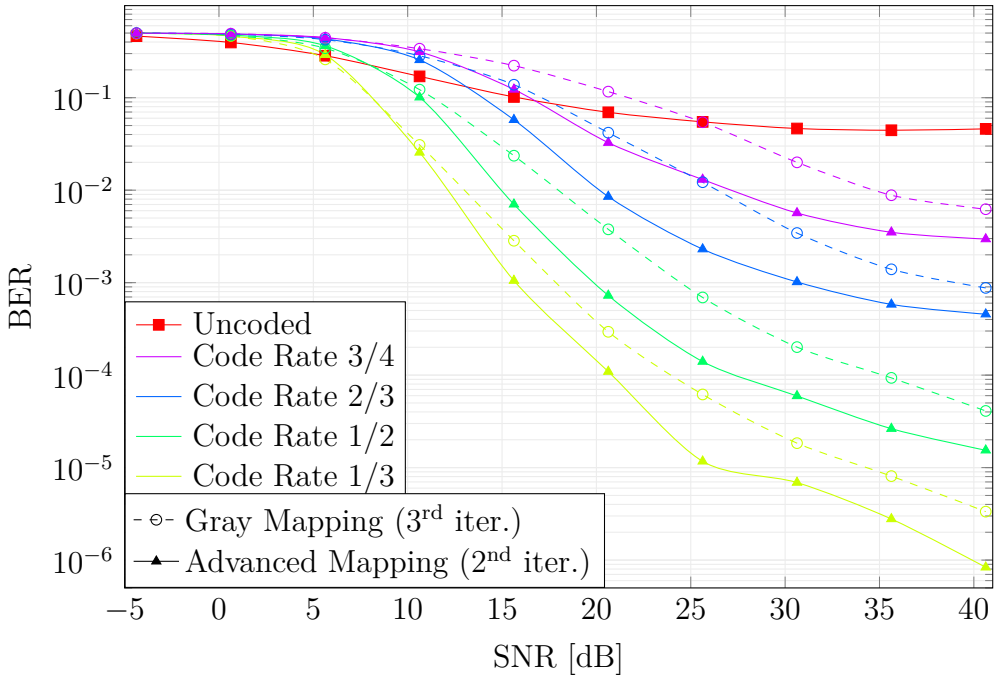

Figure 4.10: BER comparison between Gray and Advanced Mapping, $K_{cc} = 3$

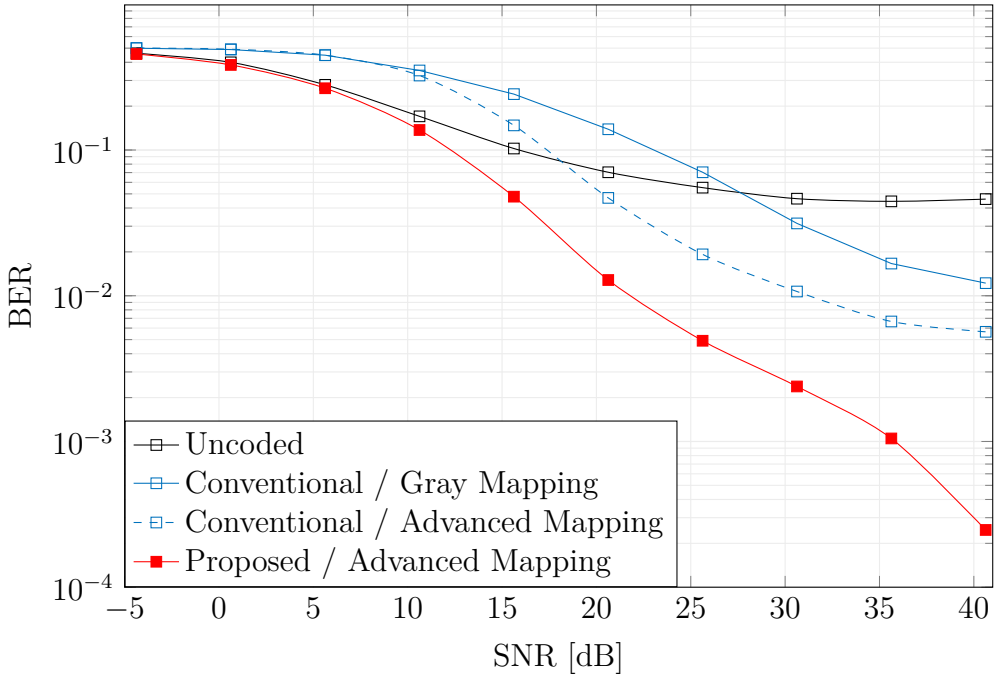

Figure 4.11: BER results for a code rate of 7/9. Performance gain due to the modified sub-channel coding scheme

5 Faster-than-Nyquist CPM

The utilization of channel coding and iterative decoding to mitigate the loss brought by the coarse quantization has been proven of benefit, but it brings considerable complexity to the receiver by aggregating two froward-backward algorithms for detection and decoding. An alternative way to deal with the problem is to dive deeper into the physical layer of the continuous phase modulation by choosing a set of parameters suited for the 1-bit ADCs at the receiver. In this chapter, a CPM waveform is introduced with a symbol duration that is only a fraction of the symbol duration of an equivalent CPFSK. The new waveform is designed with the aim of construct zero-crossings along the phase transitions, which is promising for the 1-bit quantization approach.

The proposed CPM waveform conveys the same information per time interval as the common CPFSK considered in the previous chapters, while its bandwidth can be the same or even lower. Referring to the high signaling rate, like it is typical for *faster-than-Nyquist* signaling [38], the novel waveform is termed faster-than-Nyquist continuous phase modulation (FTN-CPM). Numerical results confirm that the proposed waveform yields a significantly reduced bit error rate (BER) as compared to the existing methods [19, 20] with at least the same spectral efficiency. In addition, FTN-CPM can be detected with low-complexity and with a lower effective oversampling factor in comparison with the state-of-the-art methods.

5.1 CPM Reformulation

According to the concepts presented in Section 2.2, the CPM signal contemplates the existence of memory and, therefore, a frequency pulse larger than T_s, i.e., $L_\mathrm{cpm} > 1$, leads to the overlapping of phase transitions, which requires the system model to incorporate a state definition to describe the CPM waveform. Due to the integer nature of the CPM memory, this phase transition overlap happens in multiples of T_s. By willing to define a waveform that comply with Mazo's idea of faster-than-Nyquist signaling [38] a reformulation on the CPM phase response is proposed. The elaboration of a novel phase response function is made with aim to admit a fractional part of T_s added to length of

the frequency pulse shape. With this, the reformulation of (2-3) is given by

$$f(\tau) = \begin{cases} 0, & \text{if } \tau \leq 0, \\ \frac{1}{2}, & \text{if } \tau > T_{\text{cpm}}, \end{cases} \tag{5-1}$$

where T_{cpm} is the length of the frequency pulse. Consequently, the CPM memory is written in terms of $L_{\text{cpm}} = \lceil T_{\text{cpm}}/T_{\text{s}} \rceil$ transmit symbols, where $\lceil \cdot \rceil$ returns the smallest integer value that is bigger than or equal to the operand. The Fig. 5.1 illustrates a phase response function for the case of a rectangular frequency pulse with $T_{\text{cpm}} = 1.5\ T_{\text{s}}$ in comparison with the 1REC CPM scheme.

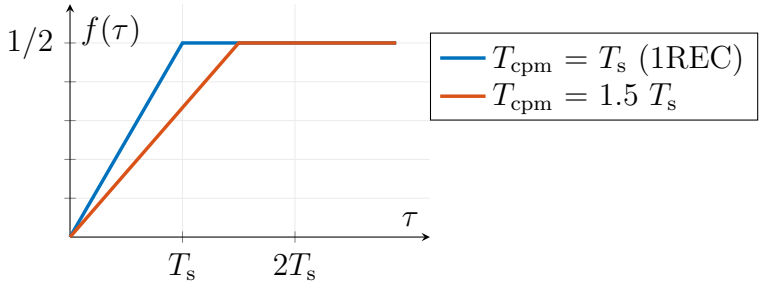

Figure 5.1: Comparison between phase responses $f(\tau)$

This formulation can be recognized as a faster-than-Nyquist approach once the signaling rate $1/T_{\text{s}}$ can become higher than the inverse of the actual phase response length $1/T_{\text{cpm}}$. Moreover, due to the fractional part of T_{s} included in T_{cpm}, a partial overlapping of the phase symbols is present, which can be identified as an ISI. To illustrate this, the phase response examples presented in Fig. 5.1 are used to construct the CPM tilted phase trellises in Fig. 5.2(a), with additional CPM parameters $M_{\text{cpm}} = 2$, $h = 1/4$, $\phi_0 = \pi/4$. Furthermore, the Fig. 5.2(b) displays the normalized power spectral density (PSD) of this case study. As expected, a longer phase transition leads to a smaller spectrum occupancy, which can possibly result in a better spectral efficiency.

5.2 Faster-than-Nyquist CPM Waveform

As known from linear modulation schemes, a faster-than-Nyquist signaling can yield a benefit for the design of zero-crossings [22], which is key for channels with 1-bit quantization at the receiver. In this section, a new subclass of CPM waveforms is introduced by using the reformulation described in the previous section, which provides relatively high, signaling rate and, potentially, high spectral efficiency at the same time. The illustrated special configurations

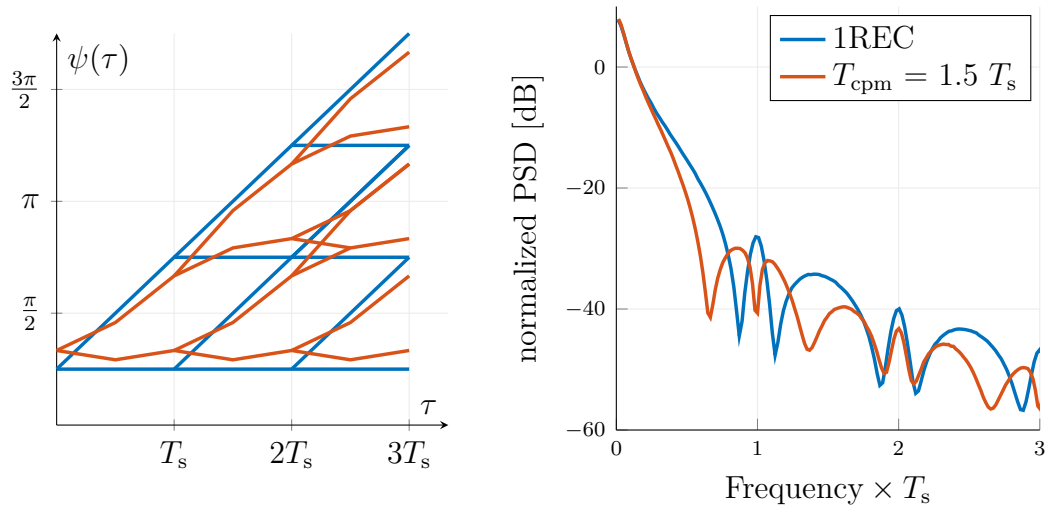

5.2(a): CPM tilted phase trellises $\psi(\tau)$ 5.2(b): PSD

Figure 5.2: Comparison with $M_{\text{cpm}} = 2$, $h = 1/4$, $\phi_0 = \pi/4$

of the proposed waveform only require low-complexity at the transmitter and receiver.

In the sequel the proposed waveform is considered with the rectangular frequency pulse with duration T_{cpm}, but the extension to frequency pulses like raised cosine and or Gaussian pulses can be done in a similar fashion. To go forward with a faster-than-Nyquist CPM definition, a bandwidth analysis is performed by using Carson's rule.

5.2.1 Proof-of-concept with Carson's Rule

The idea behind the advantages of using a novel FTN-CPM, is the that CPM signals can be constructed with significantly reduced symbol duration as compared to standard CPFSK, which convey the same information per time interval and occupy the same bandwidth. To evaluate this, spectral properties of CPM signals must be measured. Because of its mathematical tractability, Carson's bandwidth criterion, as used in [26, 39], is considered for the proof-of-concept of an FTN-CPM waveform. The generalized Carson's Rule states that the bandwidth of a frequency modulated signal $m(t)$ is described by

$$B_{\text{c}} = 2(\beta_{\text{c}} + 1)f_m, \tag{5-2}$$

where

$$\beta_{\text{c}} = h\frac{\sqrt{P_m}}{f_m}, \tag{5-3}$$

f_m is the largest "significant" frequency of $m(t)$, P_m is the power of $m(t)$ and h is the modulation index. The parameter β_c is often referred as the *effective modulation index*. To be more precise, f_m can be defined to be the one-sided effective bandwidth of $m(t)$, i.e.,

$$f_m = \frac{P_m}{2S_m(0)}, \tag{5-4}$$

where $S_m(f)$ is the PSD of $m(t)$. From (2-2), the expression of $m(t)$ for CPM signals can be written in terms of the frequency pulse g_f as

$$m(t) = \sum_{k=0}^{\infty} \alpha_k \; g_f(t - kT_s). \tag{5-5}$$

Then, by following the steps in [39], the power of $m(t)$, using i.u.d. input symbols, is expressed as

$$P_m = \frac{M_{cpm}^2 - 1}{3T_s} \int_0^{L_{cpm}T_s} g_f^2(t)dt. \tag{5-6}$$

Equation (2-3) implies that $\int_0^{L_{cpm}T_s} g_f(t)dt = 1/2$, which can be used in (5-4), which yields

$$f_m = \frac{P_m}{2S_m(0)} = \frac{6T_sP_m}{M_{cpm}^2 - 1}. \tag{5-7}$$

With this, the Carson's bandwidth in (5-2) for CPM signals can be written as

$$\begin{aligned} B_c &= 2h\sqrt{P_m} + 2f_m, \\ &= 2h\sqrt{\frac{M_{cpm}^2 - 1}{3T_s}} \left(\int_0^{L_{cpm}T_s} g_f^2(t)dt \right)^{1/2} + 4\int_0^{L_{cpm}T_s} g_f^2(t)dt, \end{aligned} \tag{5-8}$$

which can be reduced for the rectangular pulse shape as follows

$$B_c = \frac{h}{T_s}\sqrt{\frac{M_{cpm}^2 - 1}{3L_{cpm}}} + \frac{1}{L_{cpm}T_s}. \tag{5-9}$$

Apart from that, the phase shape reformulation in (5-1) can also be used for the rectangular pulse shape in (5-8), which leads to the expression

$$B_c = h\sqrt{\frac{M_{cpm}^2 - 1}{3T_sT_{cpm}}} + \frac{1}{T_{cpm}}. \tag{5-10}$$

As a reference, a standard CPFSK signal shall be considered, whose

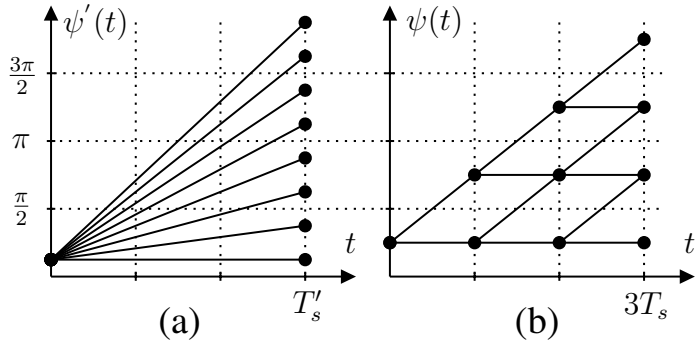

Figure 5.3: 8-symbol CPFSK (a) and three-symbol-period FTN-CPM (b) tilted trellises

parameters are indicated with $'$. The reference CPFSK is fully described by T_{s}', M_{cpm}', $h' = \frac{1}{M_{\mathrm{cpm}}'}$, $T_{\mathrm{cpm}}' = T_{\mathrm{s}}'$ and B_{c}'. Now, it is aimed to construct a FTN-CPM signal with a shorter symbol duration T_{s}, such that the ratio $T_{\mathrm{s}}'/T_{\mathrm{s}}$ is an integer value, as shown in Fig. 5.3. The conveyed information per time interval is equal for both signals in Fig. 5.3(a) and Fig. 5.3(b) by defining $M_{\mathrm{cpm}}^{T_{\mathrm{s}}'/T_{\mathrm{s}}} = M_{\mathrm{cpm}}' = 8$. With this, by using the Carson's bandwidth in (5-10), the relation between the bandwidth of the FTN-CPM signal and the reference CPFSK signal can be expressed as

$$\frac{B_{\mathrm{c}}}{B_{\mathrm{c}}'} = \frac{T_{\mathrm{s}}'}{T_{\mathrm{s}}}\left(h\sqrt{\frac{M_{\mathrm{cpm}}^2-1}{3T_{\mathrm{cpm}}/T_{\mathrm{s}}}} + \frac{T_{\mathrm{s}}}{T_{\mathrm{cpm}}}\right)\left(1+\frac{1}{M_{\mathrm{cpm}}^{T_{\mathrm{s}}'/T_{\mathrm{s}}}}\sqrt{\frac{M_{\mathrm{cpm}}^{2T_{\mathrm{s}}'/T_{\mathrm{s}}}-1}{3}}\right)^{-1}. \quad (5\text{-}11)$$

For the case of predefined design parameter $\frac{T_{\mathrm{s}}'}{T_{\mathrm{s}}}$ and M_{cpm}, the relation in (5-11)

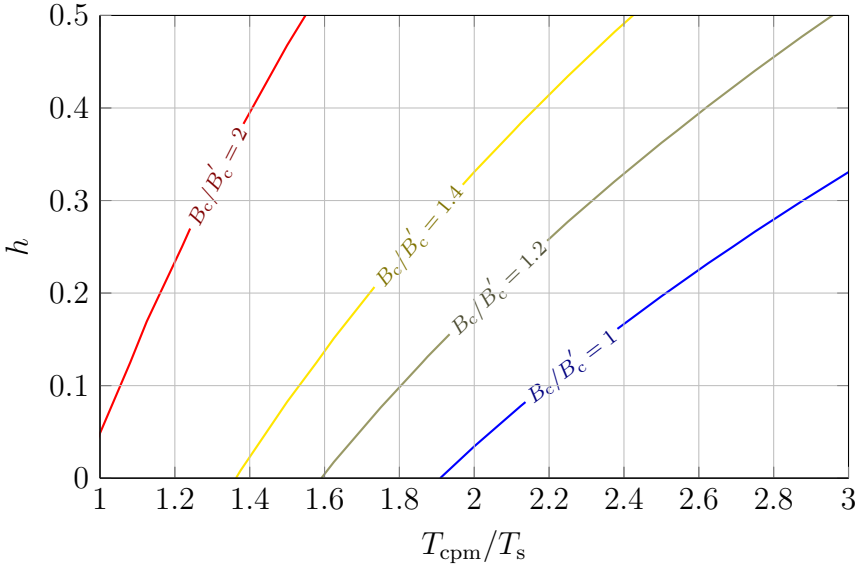

Figure 5.4: Equi-bandwidth ($B_{\mathrm{c}}/B_{\mathrm{c}}'$) lines due to Carson's criterion, $T_{\mathrm{s}}'/T_{\mathrm{s}} = 3$, $M_{\mathrm{cpm}} = 2$

is a function of modulation index h and relative frequency pulse length $T_{\mathrm{cpm}}/T_{\mathrm{s}}$. Aiming for a high spectral efficiency for the FTN-CPM signal a low relative bandwidth (5-11) is promising. An example case is illustrated for $T_{\mathrm{s}}^{'}/T_{\mathrm{s}} = 3$ and $M_{\mathrm{cpm}} = 2$ in Fig. 5.4. As can be seen, the bandwidth increase brought by the higher signaling rate can be compensated by adjustment of the modulation index h and the length of the frequency pulse T_{cpm}.

In the sequel the FTN-CPM waveform configurations are detailed which are promising in the presence of 1-bit quantization at the receiver.

5.2.2 FTN-CPM for 1-bit quantization at the receiver

A widely used waveform design criterion for channels with 1-bit quantization at the receiver is given by the maximization of distance to the decision threshold [12]. By assuming that the receive filter $g(t)$ only marginally changes the signal phase $\psi(t)$ at the receiver, zero-crossings appear whenever the phase crosses integer multiples of $\frac{\pi}{2}$. Note that the appearance of zero-crossing can be further improved by adjusting the low-IF [20]. Considering that sampling rate is equal to the FTN signaling rate, the illustrated FTN-CPM phase tree on the RHS of Fig. 5.3 is optimal in terms of distance to decision threshold, i.e., this waveform design relies on maximizing the distances between samples for the 1-bit quantization problem, which defines four phase levels. The corresponding binary FTN-CPM constellation diagram is shown in Fig. 5.5, which implies that a zero-crossing conveys the transmit symbol 1 and 0 otherwise. In order to achieve a spectral efficiency similar to the corresponding conventional CPFSK waveform, the length of the frequency pulse T_{cpm} can be increased, cf. Fig. 5.4, where different cases are examined in the sequel.

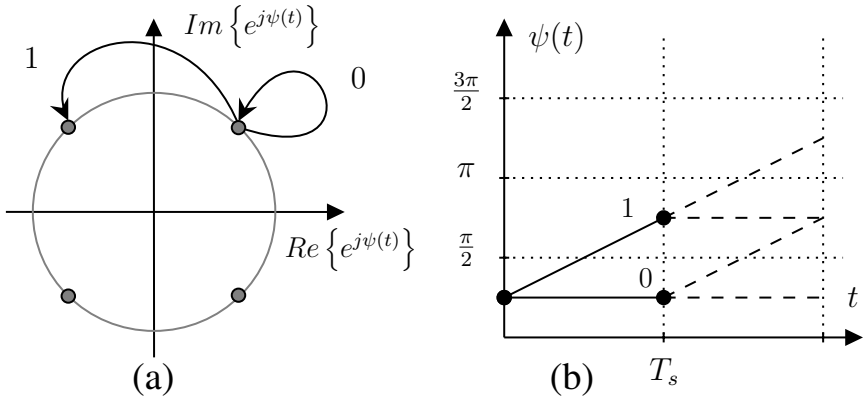

Figure 5.5: Tilted CPM constellation diagram (a) and trellis (b) of the proposed FTN-CPM with $T_{\mathrm{cpm}} = T_{\mathrm{s}}$, $h = 1/4$ and $\phi_0 = \pi/4$

5.3 A Simple Demodulation

The CPM demodulator has been discussed previously in 4.2.1, from that, an optimal receiver implemented with the BCJR algorithm becomes very complex when the modulation order M_{cpm} and the oversampling factor M increase. In order to relieve the computational load at the receiver, some versions of the proposed FTN-CPM scheme can be demodulated with an alternative simple strategy. The receive strategy for the binary FTN-CPM case with $h = \frac{1}{4}$, and sufficiently small T_{cpm}, like $T_{\text{cpm}} = 2T_{\text{s}}$, only involves the evaluation of a change in real or imaginary part, depending on the previous sample y_{k-1}, which can be cast as

$$\hat{x}_k = \begin{cases} \frac{1}{2}|\{\text{Re}\{y_k\} - \text{Re}\{y_{k-1}\}|, & \text{if } y_{k-1} \in \{1+j, -1-j\}, \\ \frac{1}{2}|\{\text{Im}\{y_k\} - \text{Im}\{y_{k-1}\}|, & \text{if } y_{k-1} \in \{1-j, -1+j\}. \end{cases} \tag{5-12}$$

Alternatively, a lookup table can also be constructed to assist the demodulation process, e.g, the Table 5.1 represents the bit decisions when y_k was received, given that y_{k-1} was the previous input to the simple demodulator. Fig. 5.6

$\mathbb{Y}_k$		y_k			
		$1+j$	$-1+j$	$-1-j$	$1-j$
y_{k-1}	$1+j$	0	1	1	0
	$-1+j$	0	0	1	1
	$-1-j$	1	0	0	1
	$1-j$	1	1	0	0

Table 5.1: Decision table for the simple receive strategy

illustrates the receiver decisions in a noise-free scenario for $T_{\text{cpm}} = T_{\text{s}}$ in Fig. 5.6(a), $T_{\text{cpm}} = 1.5T_{\text{s}}$ in Fig. 5.6(b) and $T_{\text{cpm}} = 2T_{\text{s}}$ in Fig. 5.6(c), where the phase distortion brought by the receive filter is neglected for illustration purposes. Note that for larger values for T_{cpm} the noise sensitivity increases. A special case is given by $T_{\text{cpm}} = 2T_{\text{s}}$ which results in the same number of equidistant constellation points as the corresponding 8-symbol CPFSK.

5.4 FTN-CPM results and Discussion

Table 5.2 gathers the simulation parameters for all considered CPM waveforms. 4-CPFSK [19] serves a standard reference waveform, which provides reliable communication without additional coding when considering 1-bit quantization. The same holds for 8-CPFSK [20] which serves as reference waveform that does not require additional coding for $M = 5$ and optimized low-IF with $n_{\text{IF}} = 0.25$. As it was adopted throughout this chapter, the rectangular frequency pulse is used for the CPM-FTN waveform with different durations T_{cpm},

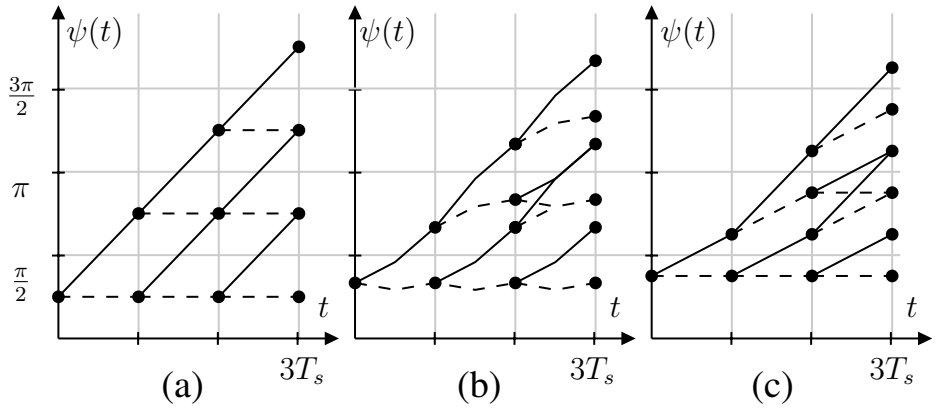

Figure 5.6: Simple receive strategy: decide for 0 (dashed line) and 1 (solid line); Different FTN-CPM configurations are shown: (a) $T_{\text{cpm}} = T_{\text{s}}$, (b) $T_{\text{cpm}} = 1.5T_{\text{s}}$ and (c) $T_{\text{cpm}} = 2T_{\text{s}}$

which goes into accordance with the CPFSK schemes that is aimed to compare it with. Moreover, the proposed FTN-CPM is represented by the running example from Section 5.2 and 5.3 specified by $M_{\text{cpm}} = 2$, $h = \frac{1}{4}$. Note that for the considered FTN-CPM schemes the receive filter is such that noise samples are uncorrelated and an auxiliary channel law (specified by N) is not required.

Waveform	Simulation Parameters
4-CPFSK [19]	$M_{\text{cpm}} = 4$, $L_{\text{cpm}} = 1$, $T_g = 0.5T_{\text{s}}$, $h = 1/4$, $n_{\text{IF}} = 0$, $\phi_0 = \pi/4$, $N = 0$
8-CPFSK [20]	$M_{\text{cpm}} = 8$, $L_{\text{cpm}} = 1$, $M = 5$, $T_g = 0.5T_{\text{s}}$, $h = 1/8$, $n_{\text{IF}} = 0.25$, $\phi_0 = \pi/8$, $N = 0$
Proposed FTN-CPM	$M_{\text{cpm}} = 2$, $M = 1$, $T_g = T_{\text{s}}$, $h = 1/4$, $n_{\text{IF}} = 0$, $\phi_0 = \pi/4$

Table 5.2: Considered waveforms

Similarly to what has been done in the Sections 4.5 and 3.4.1, the receive filter described by equation (3-27) is selected due to the maintenance of zero crossings. Additionally, the adjustable power containment bandwidth $B_{90\%}$ is considered, where we refer to 90% power containment as default and use 95% as an alternative for some cases. For consistency with the previous chapters simulations, the SNR is defined by

$$\text{SNR} = \frac{E_{\text{s}}}{N_0}(T_{\text{s}}B_{90\%})^{-1}.$$

5.4.1 Spectral Efficiency and Effective Oversampling Ratio

The spectral efficiency can be described with the ratio between the information rate the system can provide and the frequency bandwidth that the corresponding radio frequency (RF) signal occupies in the spectrum. Referring

to the 90% power containment bandwidth, it can be represented with

$$\text{spectral eff.} = \frac{I_{\text{bpcu}}}{B_{90\%}T_{\text{s}}} \leq \frac{\log_2 M_{\text{cpm}}}{B_{90\%}T_{\text{s}}} \text{ [bit/s/Hz]}, \tag{5-13}$$

where I_{bpcu} is the achievable rate with respect to one symbol duration T_{s}, which is computed by applying the methods presented in chapter 3. The effective oversampling ratio, regarding the bandwidth $B_{90\%}$, is given by

$$\text{OSR}' = M\left(B_{90\%}T_{\text{s}}\right)^{-1}. \tag{5-14}$$

Table 5.3 displays computed values for effective oversampling factor and maximum spectral efficiency for the waveforms considered in Table 5.2.

Waveform	$\frac{T_{\text{cpm}}}{T_{\text{s}}}$	M	$\frac{\log_2 M_{\text{cpm}}}{B_{90\%}T_{\text{s}}}$	$\frac{\log_2 M_{\text{cpm}}}{B_{95\%}T_{\text{s}}}$	OSR'
8-CPFSK [20]	1	5	**3.467**	**2.873**	5.778
4-CPFSK [19]	1	4	2.372	1.976	4.744
4-CPFSK [19]	1	2	2.372	1.976	2.372
Proposed FTN-CPM	1	1	2.853	1.983	2.853
Proposed FTN-CPM	1.2	1	3.079	2.176	3.079
Proposed FTN-CPM	1.4	1	3.297	2.359	3.297
Proposed FTN-CPM	1.6	1	**3.507**	2.544	3.507
Proposed FTN-CPM	1.8	1	3.691	2.720	3.691
proposed FTN-CPM	2	1	3.891	**2.881**	3.891

Table 5.3: Computed power containment bandwidths and effective oversampling factor

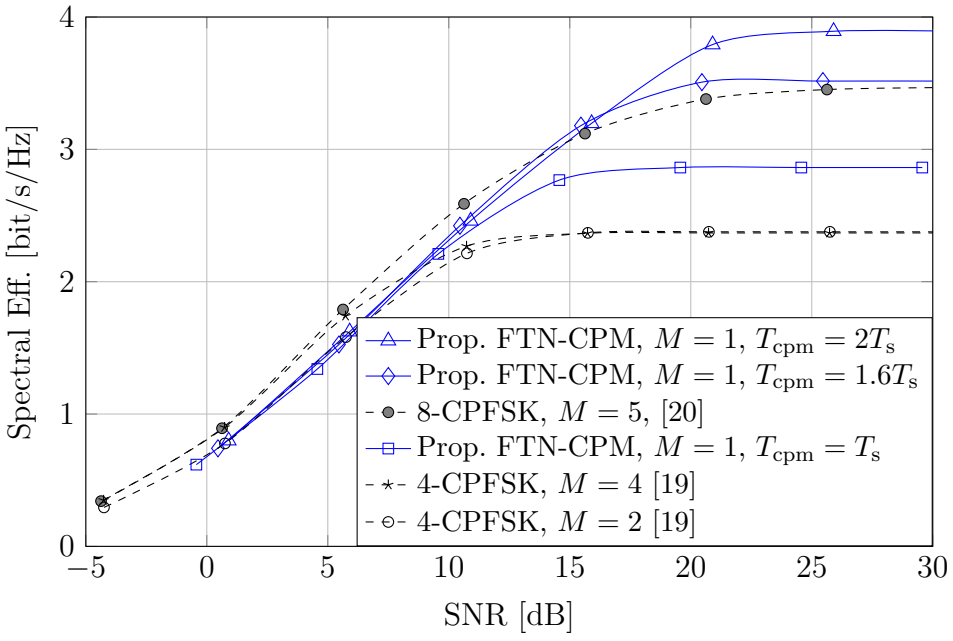

Figure 5.7: Spectral Efficiency with respect to the 90% power containment bandwidth

Moreover, Fig. 5.7 illustrates the spectrum efficiency with respect to $B_{90\%}$ versus SNR. For this bandwidth criterion choosing $T_{\text{cpm}} \geq 1.6T_{\text{s}}$ can yield a higher spectral efficiency as the corresponding CPFSK waveform for medium and high SNR. When referring to the $B_{95\%}$ it is required to choose $T_{\text{cpm}} \geq 2T_{\text{s}}$ for approaching the spectral efficiency of the corresponding CPFSK, cf. Table 5.3.

5.4.2 Bit Error Rate Results

The uncoded BER is shown in Fig. 5.8. The increase of the length of the frequency pulse T_{cpm} in the proposed binary CPM reduces the distance between the constellations points, which results in increased sensitivity to noise. Different to the 1-bit customized 8-CPFSK [20], the proposed FTN-CPM shows a BER performance which decreases fast for higher SNR. An additional highlight is that the proposed simple receiver strategy results in a BER performance which is almost identical with the performance of the optimal BCJR-based CPM demodulator especially at medium and high SNR.

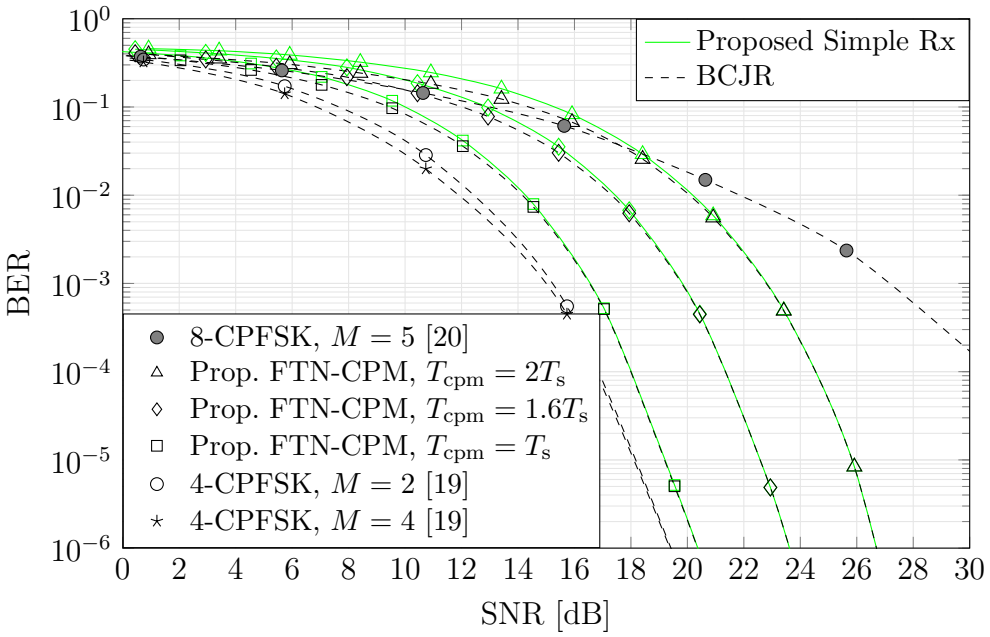

Figure 5.8: BER performance of the considered CPM waveforms

6 Adaptive Oversampling

Discretizations in sampling and quantization were first carried out in conventional forms employing a uniform partitioning of the respective domain. Later on, quantizer designs started to use nonuniform schemes, which would have the rate-distortion performance improved by taking input data statistics into account. In Bennett's work [40], the source probability distribution is considered to design a nonuniform quantization based on a companding model. Regarding the time domain, Shannon's classical uniform sampling theory detailed in [41] were also extended to nonuniform structures where the sampling-rate is adapted to an estimation of the signal bandwidth [42]. This idea is explored in [43], where a nonuniform sampling grid was designed by allocating more sampling time instances to high bandwidth signal time segments. High-rate quantization studied in [44] is associated with an adaptive sampling analysis explored in [45], which formulates optimal high-resolution sampling of one-dimensional signals, based on the MSE criterion.

In this chapter, in order to compensate for the loss in terms of the achievable rate for CPM systems with 1-bit quantization, an adaptive oversampling with respect to the signal bandwidth is considered. In this context, an MSE-based nonuniform sampling approach suited for the 1-bit quantized CPM signal is proposed. As result to the increase of the oversampling factor M, the computation complexity of the model grows reasonably high due to the exponential nature of the number of evaluations of the channel output probability, seen in equation (3-25). The nonuniform sampling scheme presented in this chapter reduces the complexity of a dense uniform sampling grid scenario by choosing appropriate samples to compose the model.

6.1 System Model Adjustment

In order to model the adaptive oversampling for the CPM scheme that was developed throughout this thesis, the discrete-time system model presented in Fig. 2.6 is adjusted.

Previously in chapter 2, a higher sampling grid has already been considered with M as the oversampling factor and D as a higher resolution multiplier. With the adaptive oversampling, the difference consists in replacing the decimation process for a sample selection strategy that aims to represent

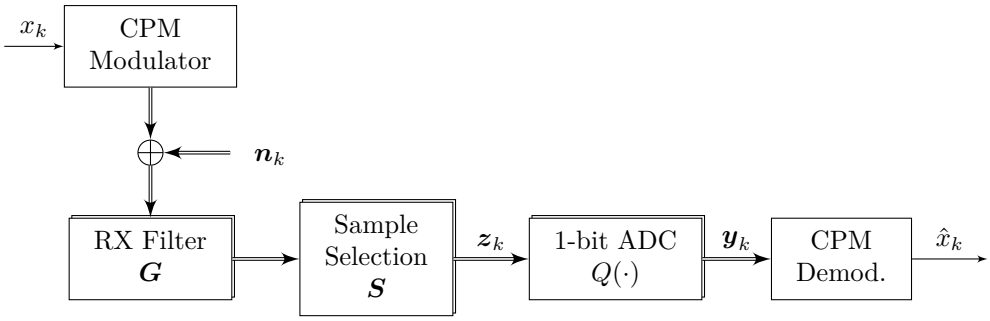

Figure 6.1: Discrete-time description of the CPM system with 1-bit quantization and adaptive oversampling at the receiver

the considered nonuniform sampling, covered in this chapter. To illustrate this idea, the discrete-time system model adjusted for adaptive oversampling is shown in Fig. 6.1.

Although the general description of the 1-bit quantized CPM signal is maintained, the nonuniform adaptive sampling needs to be detailed as part of the model. The adaptive sampling selects M_{eff} samples per symbol from the filtered received vector, where M_{eff} can be identified as an effective oversampling factor. Such operation is implemented by multiplying the filtered signal with the sample selection matrix $\boldsymbol{S}$, which has dimension $M_{\text{eff}}(\eta+1) \times MD(\eta+1)$, to be in accordance with the CPM discrete model covered in Section 2.5, and has its representation defined as follows

$$S_{i,j} = \begin{cases} 1 & \text{for } j = (\nu_i - 1)D + 1, \\ 0 & \text{otherwise,} \end{cases} \tag{6-1}$$

where the vector $[\nu_1, \ldots, \nu_{M_{\text{eff}}(\eta+1)}]^T$ is chosen such that its entries specify the indexes of the samples that will compose the resulting vector $\boldsymbol{z}_{k-\eta}^{k}$, i.e., the received samples that are input to the 1-bit quantization operation. Therefore, the received and 1-bit quantized vector $\boldsymbol{y}_{k-\eta}^{k}$ has a similar representation as compared to the equation (2-14), where the matrix $\boldsymbol{D}$ is now replaced by the matrix $\boldsymbol{S}$

$$\begin{aligned} \boldsymbol{y}_{k-\eta}^{k} &= Q\left(\boldsymbol{z}_{k-\eta}^{k}\right) \\ &= Q\left(\boldsymbol{S}\,\boldsymbol{G}\left[\sqrt{\frac{E_{\text{s}}}{T_{\text{s}}}} e^{\psi_{k-\eta-L_g}^{k}} + \boldsymbol{n}_{k-\eta-L_g}^{k}\right]\right), \end{aligned} \tag{6-2}$$

where, likewise, the quantization operator $Q(\cdot)$ is applied on each element of $\boldsymbol{z}_{k-\eta}^{k}$.

6.2 MSE Criterion for Sample Selection

Similarly to what is presented [45], this study adopts a MSE criterion to assist the decision for sampling times, which are chosen based on the quantization error averaged over all possible phase transitions. This MSE analysis is done along one symbol duration of the tilted-phase CPM signal in a noise free scenario. Let $\Psi_k(\tau)$ the tilted phase description of the CPM signal in (2-7), $0 \leq \tau < T_\mathrm{s}$, for a given state $\tilde{s}_k$, but with the extra frequency offset expressed in (2-10), i.e.,

$$\Psi_k(\tau) = \psi(\tau + kT_\mathrm{s}) + 2\pi n_\mathrm{IF}(\tau + kT_\mathrm{s})/T_\mathrm{s}.$$

With this, the tilted CPM signal that corresponds to the state $\tilde{s}_k$ is described by $\sqrt{\frac{E_s}{T_\mathrm{s}}}e^{j\Psi_k(\tau)}$, which is a complex baseband representation of a RF signal, that has the real and imaginary components separated prior to analog-to-digital conversion at the receiver. However, to deal with quantization error of complex valued signals, the absolute value operator $|\cdot|$ is considered in this analysis. Then the quantization error E_Q for both imaginary and real part of the tilted-phase CPM baseband signal can be expressed as follows

$$E_Q(k,\tau) = \sqrt{\frac{E_s}{T_\mathrm{s}}}\left| e^{j\Psi_k(\tau)} - \frac{1}{\sqrt{2}}Q\left(e^{j\Psi_k(\tau)}\right)\right|, \tag{6-3}$$

where $\frac{1}{\sqrt{2}}Q(\cdot)$ is the normalized 1-bit quantization operator applied continuously over the symbol period. The Fig. 6.2 illustrates an example of the evaluation of the quantization E_Q for two tilted CPM phase transition scenarios, both starting from the same initial phase. The first one, depicted in blue, has a lower phase increase along the symbol period T_s, i.e., it represents a lower frequency component, which causes a smaller number of phase crossings through the four-phase quantization levels established by the 1-bit quantization process. On the other hand, the second phase transition scenario, colored in red, corresponds to more quantization-level-crossings due to the higher phase increase. Moreover, this illustration shows the squared quantization error, displayed on the top, which indicates optimal sampling time instances when there is a minimum in the graph. However, the receiver does not rely on deterministic signals, thus the statistics of the CPM symbols must be considered. For a conventional approach, a uniform distribution is assumed for the input symbols. With this,

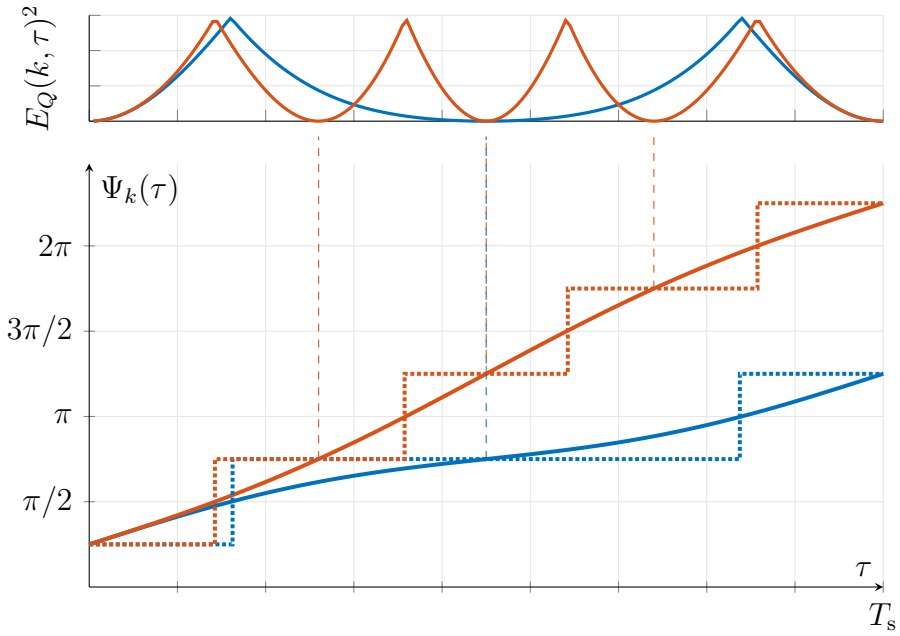

Figure 6.2: Squared quantization error of CPM tilted phase transitions

an MSE concept as function of τ is described with an average denoted by

$$\begin{aligned} \mathrm{MSE}(\tau) &= \frac{1}{n_{st}} \sum_{\tilde{s}_k} E_Q(k,\tau)^2 \\ &= \frac{1}{n_{st}} \sum_{\tilde{s}_k} \frac{E_s}{T_s} \left| e^{j\Psi_k(\tau)} - \frac{1}{\sqrt{2}} Q\left(e^{j\Psi_k(\tau)}\right) \right|^2, \end{aligned} \tag{6-4}$$

where n_{st} is the number of all possible states $\tilde{s}_k$. The expectation in performing this MSE evaluation is to identify minima that are relevant, which may be common for every tilted phase transition scenario. The next section explores this idea applied to CPM signals with raised cosine frequency pulse shape. In advance, the Fig. 6.5 represents some phase transitions of CPM signals with $M_{\mathrm{cpm}} = 8$, $h = 1/M_{\mathrm{cpm}}$, $\phi_0 = \pi/M_{\mathrm{cpm}}$, raised cosine as the frequency pulse (1RC), oversampling factor of $M = 11$, tilted with the frequency offset in (2-10) with $n_{\mathrm{IF}} = 0.25$. This scheme is also used to illustrate (6-4) with Fig. 6.6, where it is possible to identify the best sampling time instances with the minimum values of the graph.

6.3 Case Study on Raised Cosine Frequency Pulse

As proof of concept, this chapter uses the 1RC frequency pulse, illustrated in Fig. 6.3 in comparison with the 1REC frequency pulse, as a case study for two major reasons. First, the use of smooth phase transition reduces the amount of out-of-band radiation, which is a desirable feature for real-world

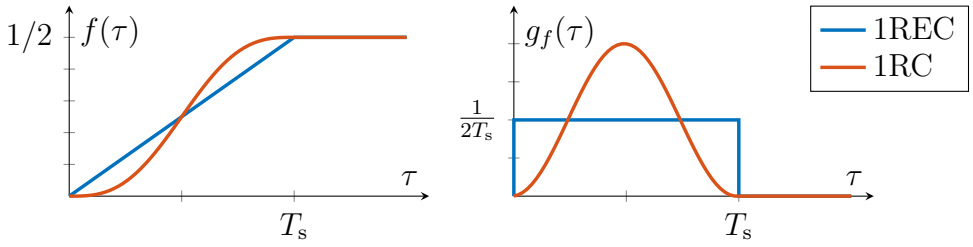

Figure 6.3: Frequency pulse shapes and their phase responses

systems. The second reason, which is a consequence of the first, consists of the presence of near-zero derivative regions of the phase response at the beginning and by the end of the phase transition. These regions present a predictable linear behavior for the tilted phase trellis for every possible phase transition. When the low-IF variable n_{IF} is adjusted, zero-crossings can be forced onto those regions. With this in mind, the estimation of an appropriate oversampling factor M and distance between the sampling time instances $d_s T_s/M$, can be done by rewriting the IF equation in (2-10) as

$$2\pi\left(\frac{h(M_{\mathrm{cpm}}-1)}{2T_s}+\frac{n_{\mathrm{IF}}}{T_s}\right)=\frac{\Delta\psi}{\Delta\tau}=\frac{2\pi h}{d_s T_s/M}, \tag{6-5}$$

where d_s is a non-negative integer and $\Delta\psi = 2\pi h$ is the minimum phase increase that would yield crossings through the 1-bit quantization decision regions, i.e., it is chosen to be the required phase shift that changes an uncertain phase level to a distinguishable one. Furthermore $2\pi h$ is the phase distance between the phase symbols in time T_s, where the quantization error evaluation (6-3) is often a minimum, vide Fig. 6.2. Equation (6-5) can be reduced to

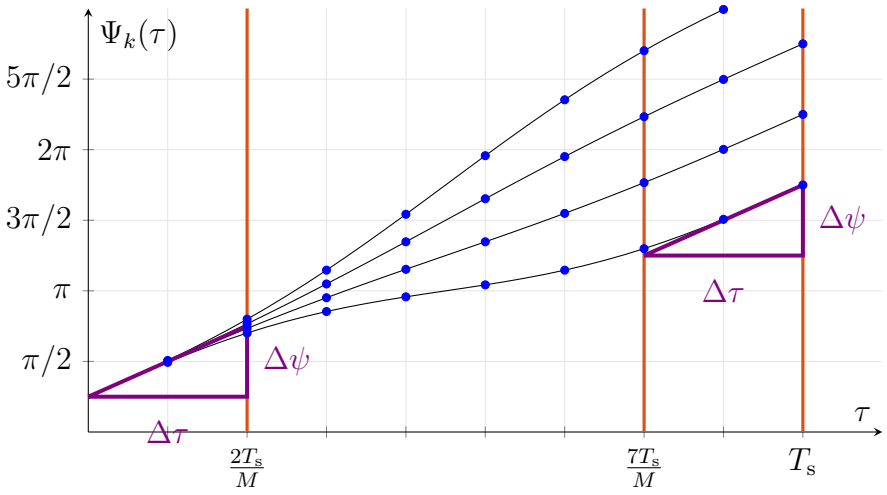

Figure 6.4: 1RC Tilted phase transitions with $M_{\mathrm{cpm}} = 4$, $h = 1/M_{\mathrm{cpm}}$, $n_{\mathrm{IF}} = 0.75$, $M = 9$

$$\frac{M}{d_s} = \frac{M_{\text{cpm}} - 1}{2} + \frac{n_{\text{IF}}}{h}, \tag{6-6}$$

where the irreducible fraction M/d_s, can be used to describe the nonuniform sampling adapted to the CPM parameters M_{cpm}, h, n_{IF}. This formulation aims to reproduce, approximately, the quantization error value in $\tau = T_{\text{s}}$, possibly a minimum, for other sampling time instances $T_{\text{s}} \pm d_s T_{\text{s}}/M$. This concept can also be used for other CPM schemes with smooth phase transitions and $L_{\text{cpm}} = 1$.

The Fig. 6.4 illustrates an example for (6-6), with $M_{\text{cpm}} = 4$, $h = 1/M_{\text{cpm}}$ and $n_{\text{IF}} = 0.75$, where the ratio M/d_s becomes $9/2$, which indicates that $M = 9$ would be an appropriate oversampling factor and the sampling instances at $2T_{\text{s}}/11$, $7T_{\text{s}}/11$ and T_{s} correspond to the samples with less quantization error. This idea can be reproduced with the case of Fig. 6.5, where $M/d_s = 11/2$, and verified with the MSE profile in Fig. 6.6. Note that in Fig. 6.5 the samples at $9T_{\text{s}}/M$ resolve all the uncertainties brought by the coarse quantization with the sample at T_{s}, i.e., it would be possible to reach the $\log_2(M_{\text{cpm}}) = 3$ bits per channel use with an effective oversampling factor $M_{\text{eff}} = 2$, using an adaptive nonuniform sampling.

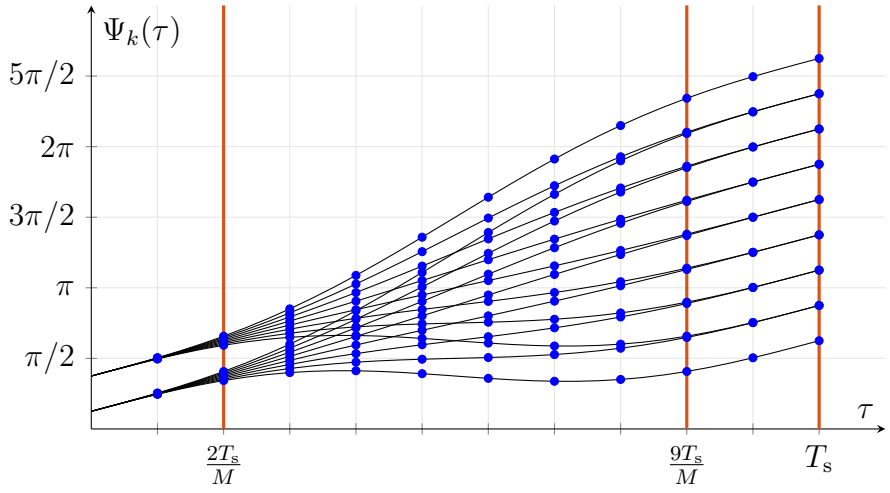

Figure 6.5: 1RC Tilted phase transitions with, $M_{\text{cpm}} = 8$, $h = 1/M_{\text{cpm}}$, $\phi_0 = \pi/M_{\text{cpm}}$, $n_{\text{IF}} = 0.25$, $M = 11$

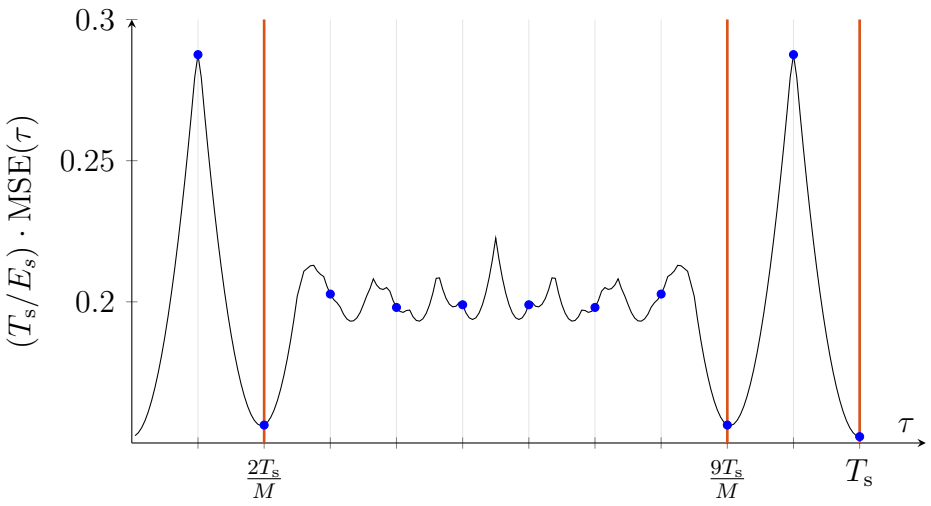

Figure 6.6: MSE profile for the scenario in Fig. 6.5

6.4 Adaptive Oversampling Results

Before presenting the simulation parameters and results, the rest of the CPM model described so far needs to be consistent with the adjustment made in Section 6.1. In order to compute the channel output probabilities with the required multivariate Gaussian integral in (3-19), the random vector $\boldsymbol{z}_{k-N}^{k}$ is now described by its mean vector and covariance matrix defined by the following

$$\boldsymbol{m}_z = \boldsymbol{S}\boldsymbol{G}\left[\sqrt{\frac{E_s}{T_s}}e^{\boldsymbol{\psi}_{k-N-L_g}^{k}}\right], \tag{6-7}$$

$$\boldsymbol{K}_z = \sigma_n^2 \boldsymbol{S}\boldsymbol{G}\boldsymbol{G}^H\boldsymbol{S}^T, \tag{6-8}$$

where $\boldsymbol{S}$ is the sample selection matrix introduced in (6-1). In the sequel the simulation parameters of the numerical results are presented

The simulations aim to show the benefit brought by the adaptive sampling over the conventional uniform sampling. With this, the considered CPM waveforms are listed below with their respective simulation parameters:

- **4-CPFSK [19] :** 1REC, $M_{\mathrm{cpm}} = 4$, $M = 3$, $n_{\mathrm{IF}} = 0$;
- **8-CPFSK [20] :** 1REC, $M_{\mathrm{cpm}} = 8$, $M = 3$ and 5, $n_{\mathrm{IF}} = 0.25$;
- **4-CPM ($M_{\mathbf{eff}} = 2$) :** 1RC, $\nu^{M_{\mathrm{eff}}} = [7, 9]^T$, $M_{\mathrm{cpm}} = 4$, $M = 9$, $n_{\mathrm{IF}} = 0.75$;
- **4-CPM ($M_{\mathbf{eff}} = 3$) :** 1RC, $\nu^{M_{\mathrm{eff}}} = [2, 7, 9]^T$, $M_{\mathrm{cpm}} = 4$, $M = 9$, $n_{\mathrm{IF}} = 0.75$;
- **8-CPM ($M_{\mathbf{eff}} = 2$) :** 1RC, $\nu^{M_{\mathrm{eff}}} = [9, 11]^T$, $M_{\mathrm{cpm}} = 8$, $M = 11$, $n_{\mathrm{IF}} = 0.25$;
- **8-CPM ($M_{\mathbf{eff}} = 3$) :** 1RC, $\nu^{M_{\mathrm{eff}}} = [2, 9, 11]^T$, $M_{\mathrm{cpm}} = 8$, $M = 11$, $n_{\mathrm{IF}} = 0.25$;

all of them with $L_{\mathrm{cpm}} = 1$, $h = 1/M_{\mathrm{cpm}}$, $\phi_0 = \pi/M_{\mathrm{cpm}}$, $N = 0$. Similar to the simulated waveforms in the previous chapter, the CPM schemes 4-CPFSK [19] and 8-CPFSK [20] serve as reference waveforms that use uniform

sampling and 1REC frequency pulse depicted in Fig. 6.3. The rest of the simulation environment is configured in an analogous way to what is considered throughout this thesis, i.e., the receive filter is assumed to be the suboptimal bandpass filter in (3-27) and the SNR definition follows the equation (3-28), with the 90% power containment bandwidth $B_{90\%}$. Subsequently, results and discussions for AIR and BER are presented.

6.4.1 Achievable Information Rate

The method to compute a lower-bound on the achievable rate is explored in Chapter 3, where an auxiliary channel law is introduced. The Fig. 6.7 illustrates how the increase of the effective oversampling factor can benefit the information rate results for the adaptive oversampling.

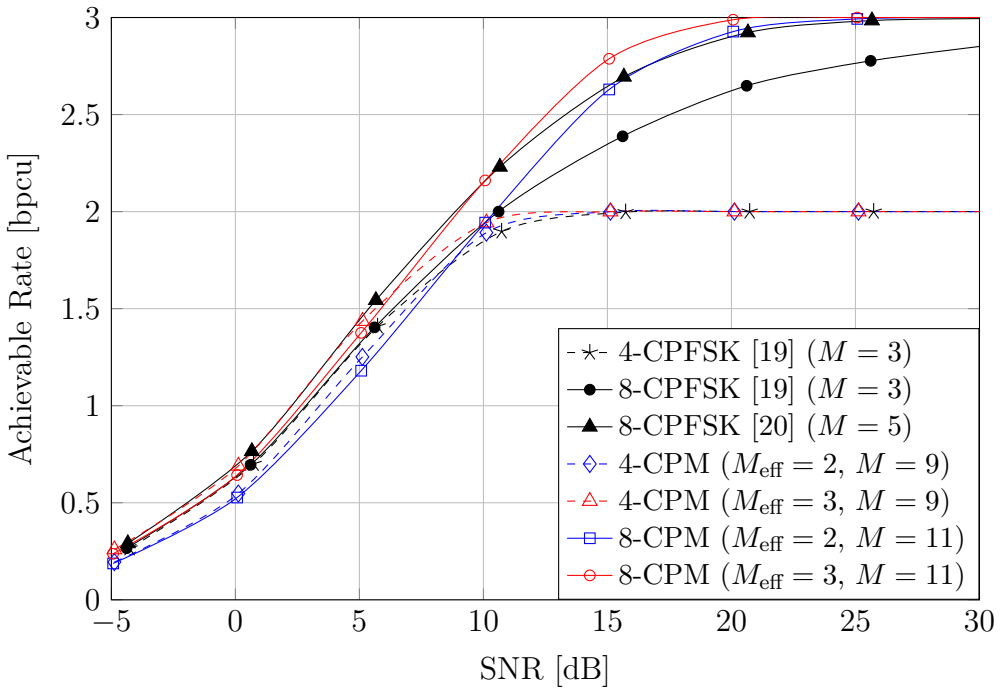

Figure 6.7: Achievable Rate of the considered CPM waveforms

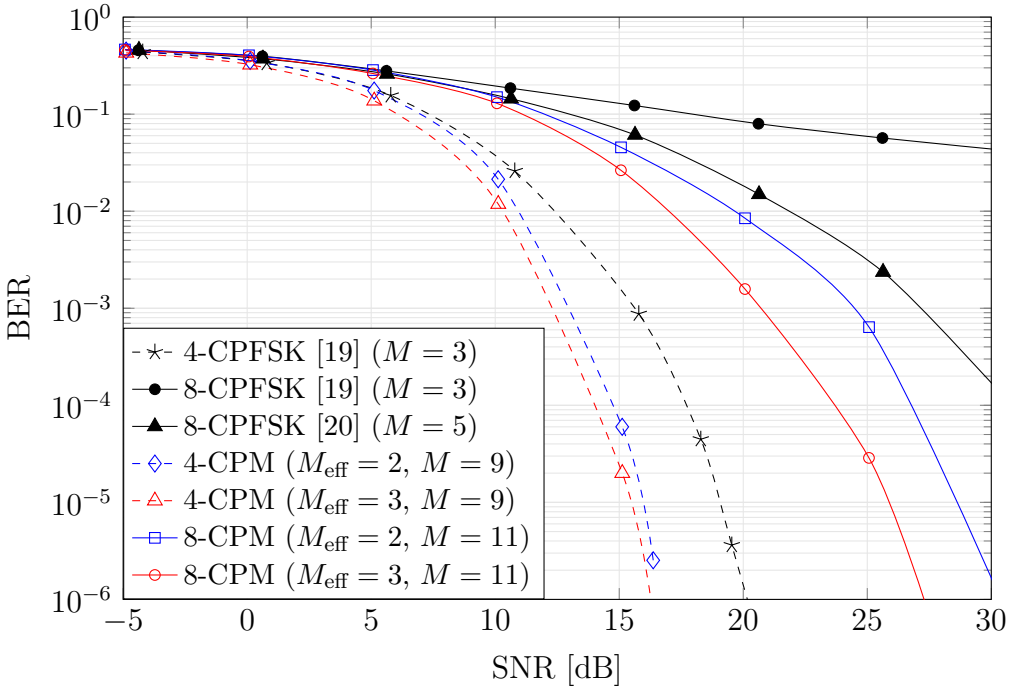

Figure 6.8: BER performance of the considered CPM waveforms

The advantage can be seen more clearly for the scenarios with $M_{\text{cpm}} = 8$, where the conventional uniform sampling is outperformed from mid to high SNR values by the nonuniform adaptive sampling. The results confirm that based on the adaptive sampling scheme the full rate of 8-CPM signals can be achieved with 2-fold oversampling ($M_{\text{eff}} = 2$) at high SNR.

6.4.2 Bit Error Rate

All BER results, from Fig. 6.8, has been computed using the BCJR algorithm that implies the auxiliary channel law presented in 4.2.1. In comparison to uniform sampling, a significant benefit can be observed when using the adaptive sampling in every considered scenario with the same or less number of sampling time instances.

7 Conclusions

Throughout this thesis, new approaches for CPM systems with 1-bit quantization at the receiver have been developed and studied. In the beginning of the thesis, the basic concepts about continuous phase modulation and some concepts from information theory are presented, with the aim to introduce the environment, part of the system description, for which the developed schemes rely on. The CPM system is modeled in a discrete-time form with 1-bit quantization and oversampling at the receiver. With analysis on the mutual information by considering an auxiliary channel law, a lower-bound on the achievable rate is computed. With this, the benefits of the oversampling and the impact of the coarse quantization were identified.

The employment of channel coding was the first idea to be conceived. An iterative detection and decoding scheme applied to the CPM system with 1-bit quantization and oversampling at the receiver has been studied. Different code rates have been considered and it turns out that channel coding is beneficial in all the cases. The bit error rate performance gain achieved by increasing the number of iterations of the turbo equalization scheme was not satisfactory, which stimulated the development of a sub-channel coding scheme. This was motivated by a deeper analysis of bit-to-symbol allocations that refers to a state-dependent bit mapping, appropriate for the 1-bit ADC problem. Then, further improvements on the BER could be obtained by using the proposed tailored bit mapping strategy in combination with a coding scheme that considers different binary sub-channels separately.

Afterwards, a subclass of CPM signals is introduced, namely CPM signals with *faster-than-Nyquist* signaling. The novel waveform is especially promising in the context of 1-bit quantization at the receiver, because it provides a good steering of zero-crossings. By considering Carson's bandwidth criterion it is shown that a waveform equivalent to common CPFSK in bandwidth and information bits per time interval can be constructed by utilizing a higher signaling rate. Numerical results show superior performance in terms of spectral efficiency and BER for the channel with 1-bit quantization at the receiver. The illustrated binary FTN-CPM signal can be detected with an extremely simple detector with a performance close to MAP detection.

Finally, this study proposes an adaptive sampling technique for CPM

signals with 1-bit quantization and oversampling. The proposed method selects appropriate sampling time instances based on an MSE criterion, which is related to the quantization error. It was shown that the frequency offset can be adjusted to induce zero-crossings and minima for quantization error. The RC frequency pulse is adopted as case study due to the smooth phase transitions. Numerical results show that the corresponding receiver with nonuniform sampling provides a better BER performance as compared to receivers with a higher complexity that use uniform sampling.

Future Work

Based on the observations and results obtained in this thesis, a wide range of future topics emerges. Regarding the iterative detection and decoding scheme presented in chapter 4, it would be interesting to evaluate additional results for modern channel coding techniques, e.g., LDPC and Polar Codes. Moreover, an IDD scheme is often suitable for a faster-than-Nyquist approach to mitigate the effects of ISI, i.e., the combined ideas presented in chapters 4 and 5 are worth investigating. Furthermore, in order to extend the concept to other frequency pulse shapes, a stronger criterion for adaptive oversampling, presented in chapter 6, needs to be developed. This work has considered 1-bit quantization with continuous phase modulation because of the energy and spectral efficiency combination in both transmit and receive chains. To leverage energy efficiency to modern communication systems with high data rate and multiple antennas, 1-bit quantization combined with constant-envelope modulations in a MIMO scenario should be investigated.

Bibliography

[1] SUNDBERG, C. E.. **Continuous phase modulation**. IEEE Commun. Mag., v. 24, n. 4, p. 25–38, April 1986.

[2] SINGH, J.; PONNURU, S. ; MADHOW, U.. **Multi-gigabit communication: the ADC bottleneck**. In: PROC. OF IEEE INTERNATIONAL CONFERENCE ON ULTRA-WIDEBAND, 2009. ICUWB 2009., p. 22–27, Vancouver, BC, Sept 2009.

[3] WALDEN, R.. **Analog-to-digital converter survey and analysis**. IEEE J. Sel. Areas Commun., v. 17, n. 4, p. 539 –550, Apr. 1999.

[4] KOCH, T.; LAPIDOTH, A.. **Increased capacity per unit-cost by oversampling**. In: PROC. OF THE IEEE CONVENTION OF ELECTRICAL AND ELECTRONICS ENGINEERS IN ISRAEL, Eilat, Israel, Nov. 2010.

[5] GREWAL, H.. **Oversampling the ADC12 for higher resolution**. Texas Instruments: Application Report, July 2006.

[6] GILBERT, E. N.. **Increased information rate by oversampling**. IEEE Trans. Inf. Theory, v. 39, n. 6, p. 1973–1976, Nov 1993.

[7] SHAMAI (SHITZ), S.. **Information rates by oversampling the sign of a bandlimited process**. IEEE Trans. Inf. Theory, v. 40, n. 4, p. 1230–1236, July 1994.

[8] ZAKAI, M.. **Band-limited functions and the sampling theorem**. Information and Control, v. 8, n. 2, p. 143 – 158, 1965.

[9] LANDAU, L.; DÖRPINGHAUS, M. ; FETTWEIS, G. P.. **1-bit quantization and oversampling at the receiver: Communication over bandlimited channels with noise**. IEEE Commun. Lett., v. 21, n. 5, p. 1007–1010, May 2017.

[10] ZHANG, W.. **A general framework for transmission with transceiver distortion and some applications**. IEEE Trans. Commun., v. 60, n. 2, p. 384–399, Feb. 2012.

[11] BENDER, S.; DÖRPINGHAUS, M. ; FETTWEIS, G. P.. **On the achievable rate of bandlimited continuous-time 1-bit quantized AWGN channels**. In: PROC. IEEE INT. SYMP. INFORM. THEORY (ISIT), p. 2083–2087, Aachen, Germany, 2017.

[12] LANDAU, L.; KRONE, S. ; FETTWEIS, G. P.. **Intersymbol-interference design for maximum information rates with 1-bit quantization and oversampling at the receiver**. In: PROC. OF THE INTERNATIONAL ITG CONFERENCE ON SYSTEMS, COMMUNICATIONS AND CODING, Munich, Germany, Jan. 2013.

[13] GOKCEOGLU, A.; BJÖRNSON, E.; LARSSON, E. G. ; VALKAMA, M.. **Waveform design for massive MISO downlink with energy-efficient receivers adopting 1-bit ADCs**. In: PROC. IEEE INT. CONF. COMMUN. (ICC), p. 1–7, Kuala Lumpur, Malaysia, May 2016.

[14] JACOBSSON, S.; DURISI, G.; COLDREY, M.; GUSTAVSSON, U. ; STUDER, C.. **Throughput analysis of massive MIMO uplink with low-resolution ADCs**. v. 16, n. 6, p. 4038–4051, June 2017.

[15] GOKCEOGLU, A.; BJÖRNSON, E.; LARSSON, E. G. ; VALKAMA, M.. **Spatio-temporal waveform design for multi-user massive MIMO downlink with 1-bit receivers**. IEEE Journal of Selected Topics in Signal Processing, v. 11, n. 2, p. 347–362, Mar. 2017.

[16] ÜÇÜNCÜ, A. B.; YILMAZ, A. Ö.. **Oversampling in one-bit quantized massive MIMO systems and performance analysis**. v. 17, n. 12, p. 7952–7964, Dec. 2018.

[17] SHAO, Z.; LANDAU, L. T. N. ; DE LAMARE, R. C.. **Channel estimation using 1-bit quantization and oversampling for large-scale multiple-antenna systems**. In: PROC. IEEE INT. CONF. ACOUST., SPEECH, SIGNAL PROCESS., p. 4669–4673, Brighton, United Kingdom, 2019.

[18] SHAO, Z.; DE LAMARE, R. C. ; LANDAU, L. T. N.. **Iterative detection and decoding for large-scale multiple-antenna systems with 1-bit ADCs**. IEEE Wireless Communications Letters, v. 7, n. 3, p. 476–479, June 2018.

[19] LANDAU, L. T. N.; DÖRPINGHAUS, M.; DE LAMARE, R. C. ; FETTWEIS, G. P.. **Achievable rate with 1-bit quantization and oversampling**

using continuous phase modulation-based sequences. IEEE Trans. Wireless Commun., v. 17, n. 10, p. 7080–7095, Oct 2018.

[20] BENDER, S.; DÖRPINGHAUS, M. ; FETTWEIS, G. P.. **The potential of continuous phase modulation for oversampled 1-bit quantized channels**. In: PROC. OF THE IEEE INT. WORKSHOP ON SIGNAL PROCESSING ADVANCES IN WIRELESS COMMUNICATIONS, Cannes, France, July 2019.

[21] ANDERSON, J.; AULIN, T. ; SUNDBERG, C. E.. **Digital Phase Modulation**. Plenum Press, New York, 1986.

[22] LANDAU, L. T. N.; DÖRPINGHAUS, M. ; FETTWEIS, G. P.. **1-bit quantization and oversampling at the receiver: Sequence-based communication**. EURASIP J. Wireless Commun. Netw., v. 17, n. 83, 2018.

[23] RIMOLDI, B. E.. **A decomposition approach to CPM**. IEEE Trans. Inf. Theory, v. 34, n. 2, p. 260–270, Mar. 1988.

[24] SCHOLAND, T.; JUNG, P.. **Intermediate frequency zero-crossing detection of filtered MSK based on irregular sampling**. European Trans. on Telecommunications, v. 18, n. 7, p. 669–683, 2007.

[25] SHANNON, C. E.. **A mathematical theory of communications**. Bell System Technical Journal, v. 27, p. 379–423, July 1948.

[26] BARBIERI, A.; CERO, A.; PIEMONTESE, A. ; COLAVOLPE, G.. **Markov capacity of continuous phase modulations**. In: PROC. IEEE INT. SYMP. INFORM. THEORY (ISIT), p. 161–165, Nice, France, June 2007.

[27] ARNOLD, D. M.; LOELIGER, H.-A.; VONTOBEL, P. O.; KAVCIC, A. ; ZENG, W.. **Simulation-based computation of information rates for channels with memory**. IEEE Trans. Inf. Theory, v. 52, n. 8, p. 3498–3508, Aug. 2006.

[28] BAHL, L.; COCKE, J.; JELINEK, F. ; RAVIV, J.. **Optimal decoding of linear codes for minimizing symbol error rate (corresp.)**. IEEE Trans. Inf. Theory, v. 20, n. 2, p. 284–287, Mar. 1974.

[29] GENZ, A.. **Numerical computation of multivariate normal probabilities**. Journal of Computational and Graphical Statistics, p. 141–149, 1992.

[30] LANDAU, L.; DÖRPINGHAUS, M.; DE LAMARE, R. C. ; FETTWEIS, G. P.. **Achievable rate with 1-bit quantization and oversampling at the receiver using continuous phase modulation**. In: PROC. OF THE IEEE INT. CONF. ON UBIQUITOUS WIRELESS BROADBAND, Salamanca, Spain, Sept. 2017.

[31] COSTA, M. H. M.. **A practical demodulator for continuous phase modulation**. In: PROC. IEEE INT. SYMP. INFORM. THEORY (ISIT), p. 88, Trondheim, Norway, Jun 1994.

[32] HAGENAUER, J.; OFFER, E. ; PAPKE, L.. **Iterative decoding of binary block and convolutional codes**. IEEE Trans. Inf. Theory, v. 42, n. 2, p. 429–445, Mar. 1996.

[33] BERROU, C.; GLAVIEUX, A. ; THITIMAJSHIMA, P.. **Near shannon limit error-correcting coding and decoding: Turbo-codes**. In: PROC. IEEE INT. CONF. COMMUN. (ICC), vol. 2, p. 1064–1070, Geneva, Switzerland, May 1993.

[34] DOUILLARD, C.; JEZEQUEL, M. ; BERROU, C.. **Iterative correction of intersymbol interference: Turbo equalization**. European Trans. on Telecommunications, v. 6, n. 5, p. 507–511, 1995.

[35] TÜCHLER, M.; SINGER, A. C.. **Turbo equalization: An overview**. IEEE Trans. Inf. Theory, v. 57, n. 2, p. 920–952, Jan. 2011.

[36] FORNEY, G. D.. **Convolutional codes i: Algebraic structure**. IEEE Trans. Inf. Theory, v. 16, n. 6, p. 729–738, Nov. 1970.

[37] CAIN, J. B.; CLARK, G. C. ; GEIST, J. M.. **Punctured convolutional codes of rate (n - 1)/n and simplifed maximum likelihood decoding**. IEEE Trans. Inf. Theory, v. 25, n. 1, p. 97–100, Jan. 1979.

[38] MAZO, J. E.. **Faster-than-Nyquist signaling**. Bell System Technical Journal, v. 54, n. 1, p. 1451–1462, Oct. 1975.

[39] CHUN-HSUAN KUO; CHUGG, K. M.. **On the bandwidth efficiency of CPM signals**. In: PROC. IEEE MILITARY COMMUNICATIONS CONFERENCE (MILCOM), vol. 1, p. 218–224, Oct 2004.

[40] BENNET, W. R.. **Spectra of quantized signals**. Bell System Technical Journal, v. 27, n. 3, p. 446–472, 1948.

[41] JERRI, A. J.. **The Shannon sampling theorem — its various extensions and applications: A tutorial review**. Proceedings of the IEEE, v. 65, n. 11, p. 1565–1596, 1977.

[42] HORIUCHI, K.. **Sampling principle for continuous signals with time-varying bands**. Information and Control, v. 13, n. 1, p. 53–61, 1968.

[43] CLARK, J.; PALMER, M. ; LAWRENCE, P.. **A transformation method for the reconstruction of functions from nonuniformly spaced samples**. IEEE Trans. on Acoustics, Speech and Signal Processing, v. 55, n. 2, p. 1151–1165, 1985.

[44] GRAY, R. M.; NEUHOFF, D. L.. **Quantization**. IEEE Trans. Inf. Theory, v. 44, n. 6, p. 2325–2383, Oct 1998.

[45] DAR, Y.; BRUCKSTEIN, A. M.. **On high-resolution adaptive sampling of deterministic signals**. Journal of Mathematical Imaging and Vision, v. 61, n. 7, p. 944–966, 2019.

A Published paper

The paper *Continuous Phase Modulation with 1-bit Quantization and Oversampling Using Iterative Detection and Decoding* was presented at the Asilomar Conference on Signals, Systems, and Computers, ACSSC 2019. The paper was accepted for oral presentation on November 3-6, 2019 in Pacific Grove, CA, USA.

The paper *Continuous Phase Modulation with Faster-than-Nyquist Signaling for Channels With 1-bit Quantization and Oversampling at the Receiver* has been submitted to the Asilomar Conference on Signals, Systems, and Computers, ACSSC 2020. The paper was accepted for video presentation on November 1-4, 2020 in Pacific Grove, CA, USA.

The paper *Continuous Phase Modulation with 1-bit Quantization and Oversampling Using Iterative Detection and Decoding* has been submitted to the EURASIP Journal on Wireless Communications and Networking, and is currently under review.